

AD-A171 396

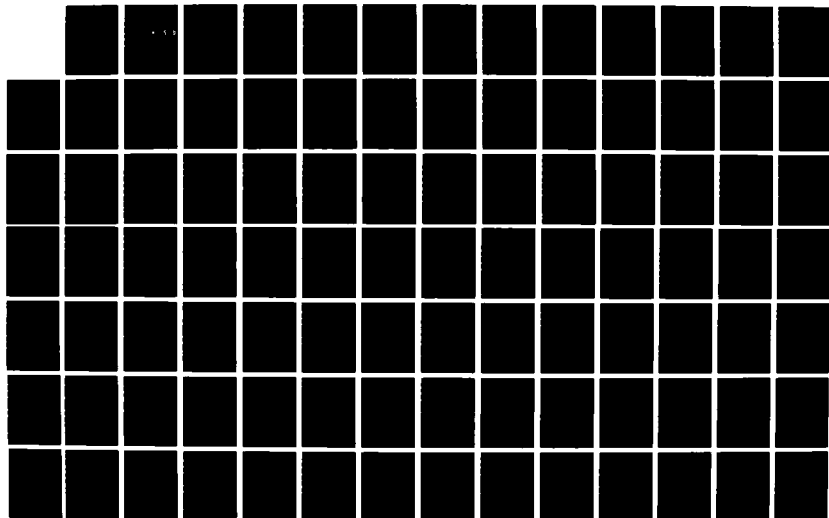
TWO-DIMENSIONAL BEAMFORMING USING A FREQUENCY DOMAIN  
COMPLEX LEAST MEAN-SQUARES (LMS) ADAPTIVE FILTER(U)  
NAVAL POSTGRADUATE SCHOOL MONTEREY CA F CHAN JUN 86

1/2

UNCLASSIFIED

F/G 9/5

ML





MI

No.

AD-A171 396

NAVAL POSTGRADUATE SCHOOL  
Monterey, California



DTIC  
ELECTE  
SEP 05 1986  
S D  
D

THESIS

TWO-DIMENSIONAL BEAMFORMING USING A  
FREQUENCY DOMAIN COMPLEX LEAST MEAN-  
SQUARES (LMS) ADAPTIVE FILTER

by

Francis Chan

June 1986

Thesis Advisor: Lawrence J. Ziomek

Approved for public release; distribution is unlimited.

DTIC FILE COPY

UNCLASSIFIED

SECURITY CLASSIFICATION OF THIS PAGE

AD-A171 396

## REPORT DOCUMENTATION PAGE

1a REPORT SECURITY CLASSIFICATION UNCLASSIFIED			1b. RESTRICTIVE MARKINGS		
2a SECURITY CLASSIFICATION AUTHORITY			3 DISTRIBUTION/AVAILABILITY OF REPORT Approved for public release; distribution is unlimited.		
2b. DECLASSIFICATION/DOWNGRADING SCHEDULE					
4 PERFORMING ORGANIZATION REPORT NUMBER(S)			5. MONITORING ORGANIZATION REPORT NUMBER(S)		
6a. NAME OF PERFORMING ORGANIZATION Naval Postgraduate School		6b OFFICE SYMBOL (If applicable) Code 62		7a. NAME OF MONITORING ORGANIZATION Naval Postgraduate School	
6c. ADDRESS (City, State, and ZIP Code) Monterey, California 93943-5000				7b. ADDRESS (City, State, and ZIP Code) Monterey, California 93943-5000	
8a NAME OF FUNDING/SPONSORING ORGANIZATION		8b. OFFICE SYMBOL (If applicable)		9. PROCUREMENT INSTRUMENT IDENTIFICATION NUMBER	
8c. ADDRESS (City, State, and ZIP Code)				10 SOURCE OF FUNDING NUMBERS	
		PROGRAM ELEMENT NO		PROJECT NO	TASK NO
				WORK UNIT ACCESSION NO	
11 TITLE (Include Security Classification) TWO-DIMENSIONAL BEAMFORMING USING A FREQUENCY DOMAIN COMPLEX LEAST MEAN-SQUARES (LMS) ADAPTIVE FILTER					
12 PERSONAL AUTHOR(S) Chan, Francis					
13a TYPE OF REPORT Master's Thesis		13b TIME COVERED FROM TO		14 DATE OF REPORT (Year, Month, Day) 1986, June	
15 PAGE COUNT 138					
16 SUPPLEMENTARY NOTATION					
17 COSATI CODES			18 SUBJECT TERMS (Continue on reverse if necessary and identify by block number)		
FIELD	GROUP	SUB-GROUP	Array Processing; Adaptive Spatial Resolution; Two-Dimensional Array, Sonar Signal Processing; Beamforming		
19 ABSTRACT (Continue on reverse if necessary and identify by block number)  The complex LMS adaptive algorithm developed by Widrow [Ref. 1] is used in the frequency domain to estimate the azimuth and elevation angles of a plane wave incident upon a planar array. The complex LMS algorithm is applied to two cases. The first case is a passive detection problem. The second case is a pulse communication problem. In both cases, complex weights are determined using the complex LMS algorithm which cophase all of the output electrical signals from the planar array. Three versions of the complex LMS algorithm are studied and their performances are compared.					
20 DISTRIBUTION/AVAILABILITY OF ABSTRACT <input checked="" type="checkbox"/> UNCLASSIFIED/UNLIMITED <input type="checkbox"/> SAME AS RPT <input type="checkbox"/> DTIC USERS				21 ABSTRACT SECURITY CLASSIFICATION Unclassified	
22a NAME OF RESPONSIBLE INDIVIDUAL Prof. Lawrence J. Ziomek				22b TELEPHONE (Include Area Code) (408) 646-3206	
				22c OFFICE SYMBOL Code Zm	

Approved for public release; distribution is unlimited.

Two-Dimensional Beamforming Using a Frequency Domain  
Complex Least Mean-Square (LMS) Adaptive Filter

by

Francis Chan  
Lieutenant, United States Navy  
B.S., The University of Rochester, 1979

Submitted in partial fulfillment of the  
requirements for the degrees of

MASTER OF SCIENCE IN ELECTRICAL ENGINEERING

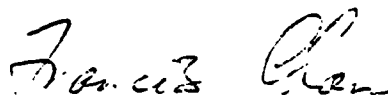
and

ELECTRICAL ENGINEER

from the

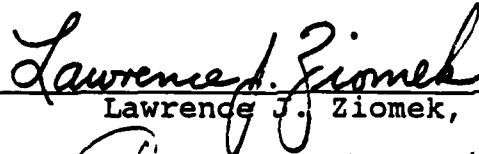
NAVAL POSTGRADUATE SCHOOL  
June 1986

Author:

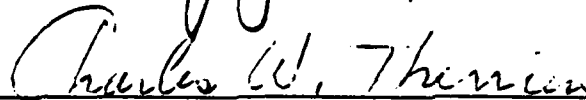


Francis Chan

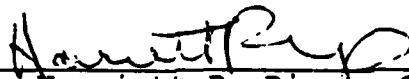
Approved by:



Lawrence J. Ziomek, Thesis Advisor



Charles W. Therrien, Second Reader



Harriett B. Rigas, Chairman,  
Department of Electrical and Computer Engineering



J. N. Dyer,  
Dean of Science and Engineering

# ABSTRACT

The complex LMS adaptive algorithm developed by Widrow [Ref. 1] is used in the frequency domain to estimate the azimuth and elevation angles of a plane wave incident upon a planar array. The complex LMS algorithm is applied to two cases. The first case is a passive detection problem. The second case is a pulse communication problem. In both cases, complex weights are determined using the complex LMS algorithm which cophase all of the output electrical signals from the planar array. Three versions of the complex LMS algorithm are studied and their performances are compared.



Accession For	
NTIS CRA&I	<input checked="checked" type="checkbox"/>
DTIC TAB	<input type="checkbox"/>
Unannounced	<input type="checkbox"/>
Justification	
By	
Distribution/	
Availability Codes	
Dist	Avail and/or Special
A-1	

## TABLE OF CONTENTS

I.	INTRODUCTION -----	11
II.	THEORY OF SYSTEM MODEL -----	17
A.	OVERVIEW OF ARRAYS -----	17
1.	Linear Arrays -----	17
2.	Planar Arrays -----	21
B.	THE PLANE WAVE MODEL -----	29
1.	Far-Field Condition -----	29
2.	Propagation of a Plane Wave from a Far-Field Source -----	31
C.	FREQUENCY DOMAIN LMS ADATIVE FILTER FOR SPATIAL RESOLUTION -----	34
1.	Phase Weights for the Planar Array -----	34
2.	The Frequency Domain LMS Adaptive Filter -----	37
3.	Applying the Frequency Domain LMS Adaptive Filter to a Planar Array -----	41
a.	Orthogonal Linear Arrays -----	42
b.	Two-dimensional Array -----	44
c.	Separable Two-dimensional Array -----	45
4.	Extracting Estimates of the Direction Cosines u and v from Phase Weights -----	46
a.	Direction Cosine Estimates for Linear Arrays -----	47
b.	Direction Cosine Estimates for Planar Arrays -----	49
5.	Unwrapping the Steering Phase Weights ---	51

a.	Linear Array Unwrapping -----	51
b.	Two-dimensional Array Unwrapping ----	60
6.	Summary -----	66
D.	NOISE MODEL -----	66
III.	LOW FREQUENCY PASSIVE SONAR TARGET LOCALIZATION -	68
A.	PROBLEM STATEMENT -----	69
B.	SIMULATION -----	71
C.	RESULTS -----	74
1.	Orthogonal Linear Arrays -----	75
2.	Two-dimensional Array -----	78
3.	Two-dimensional Array with Separable Weights -----	84
D.	SUMMARY -----	88
IV.	PULSE COMMUNICATION -----	91
A.	TRANSMIT WAVEFORMS -----	94
1.	Rectangular-Envelope CW Pulse -----	94
2.	Rectangular-Envelope LFM Pulse -----	95
B.	PROBLEM STATEMENT -----	96
C.	RESULTS -----	98
1.	Homogeneous Case -----	98
2.	Inhomogeneous Case -----	103
D.	SUMMARY -----	104
V.	CONCLUSIONS AND RECOMMENDATIONS -----	110
APPENDIX A:	THE FREQUENCY DOMAIN LMS ADAPTIVE ALGORITHM -----	113
APPENDIX B:	DESCRIPTION OF SIMULATION PROGRAM FOR THE PASSIVE DETECTION CASE -----	124

APPENDIX C: DESCRIPTION OF SIMULATION PROGRAM FOR THE PULSE COMMUNICATION CASE -----	132
LIST OF REFERENCES -----	135
INITIAL DISTRIBUTION LIST -----	137

# LIST OF TABLES

1.	PHASE WEIGHTS FOR BEAMSTEERING -----	52
2.	PHASE UNWRAPPING -----	57
3.	DESIRED PHASE WEIGHTS $\{\xi(m,n)\}$ GIVEN THAT $u = -0.7, v = +0.7$ -----	62
4.	OBSERVED PHASES OF THE STEADY STATE ADAPTIVE WEIGHTS $\{\xi'(m,n)\}$ -----	62
5.	UNWRAP FACTORS $\{w(m,n)\}$ -----	63
6.	SUMMARY OF COMPLEX LMS ADAPTIVE FILTER PERFORMANCE FOR THE ORTHOGONAL LINEAR ARRAY CONFIGURATION AT SNR = 0 dB -----	80
7.	SUMMARY OF COMPLEX LMS ADAPTIVE FILTER PERFORMANCE FOR THE TWO-DIMENSIONAL ARRAY AT SNR = 0 dB -----	84
8.	SUMMARY OF COMPLEX LMS ADAPTIVE FILTER PERFORMANCE FOR THE TWO-DIMENSIONAL ARRAY WITH SEPARABLE WEIGHTS AT SNR = 0 dB -----	88
9.	PERFORMANCE OF COMPLEX LMS ADAPTIVE FILTER FOR SPATIAL RESOLUTION, 100 ITERATIONS, INPUT SNR = 0 dB FOR CW PULSE, HOMOGENEOUS CASE -----	99
10.	PERFORMANCE OF COMPLEX LMS ADAPTIVE FILTER FOR SPATIAL RESOLUTION, 100 ITERATIONS, INPUT SNR = 0 dB FOR LFM PULSE, HOMOGENEOUS CASE -----	100
11.	PERFORMANCE OF COMPLEX LMS ADAPTIVE FILTER FOR SPATIAL RESOLUTION, 100 ITERATIONS, INPUT SNR = 0 dB FOR CW PULSE, INHOMOGENECUS CASE -----	105
12.	PERFORMANCE OF COMPLEX LMS ADAPTIVE FILTER FOR SPATIAL RESOLUTION, 100 ITERATIONS, INPUT SNR = 0 dB, LFM PULSE, INHOMOGENEOUS CASE -----	107

## LIST OF FIGURES

1.	Frequency Domain Adaptive Array -----	15
2.	A Seven-Element Linear Array with Uniform Interelement Spacing and Point Source Elements ----	18
3.	Directivity Pattern of a Three-Element Linear Array -----	22
4.	Directivity Pattern of a Four-Element Linear Array -----	22
5.	Directivity Pattern of a Seven-Element Linear Array for $d/\lambda = 0.1$ -----	23
6.	Directivity Pattern of a Seven-Element Linear Array for $d/\lambda = 0.2$ -----	23
7.	Directivity Pattern of a Seven-Element Linear Array for $d/\lambda = 0.5$ -----	24
8.	Directivity Pattern of a Seven-Element Linear Array for $d = \lambda$ -----	25
9.	Beamsteering by Applying a Linear Phase Shift Across the Array -----	26
10.	Steered Directivity Pattern -----	27
11.	Sensor Element Arrangement of a Rectangular Planar Array -----	30
12.	Transformation From Spherical Coordinate Space to Direction Cosine Space -----	30
13.	Adaptive Cophasing Scheme for a Linear Array -----	35
14.	A Particular Orthogonal Linear Arrays Configuration -----	43
15.	Phase Angles for Beamsteering -----	55
16.	Wrapped-Around Phase Angles -----	56
17.	System Geometry -----	70

18.	Logical Flow Graph of the Simulation Program for the Low Frequency Passive Detection Problem ---	72
19.	Convergence Characteristics of the LMS Adaptive Filter using the Orthogonal Linear Arrays Configuration in Estimating the Direction Cosine u at an Input SNR of 0 dB -----	76
20.	Convergence Characteristics of the LMS Adaptive Filter using the Orthogonal Linear Arrays Configuration in Estimating the Direction Cosine v at an Input SNR of 0 dB -----	77
21.	The RMS Error in Estimating u and v using the Orthogonal Linear Arrays Configuration at an Input SNR of 0 dB -----	79
22.	Convergence Characteristics of the LMS Adaptive Filter for the Two-dimensional Array in Estimating the Direction Cosine u at an Input SNR of 0 dB -----	81
23.	Convergence Characteristics of the LMS Adaptive Filter for the Two-dimensional Array in Estimating the Direction Cosine v at an Input SNR of 0 dB -----	82
24.	The RMS Error in Estimating u and v using the Two-dimensional Array at an Input SNR of 0 dB -----	83
25.	Convergence Characteristics of the LMS Adaptive Filter for the Two-dimensional Array with Separable Weights in Estimating the Direction Cosine u at an Input SNR of 0 dB -----	85
26.	Convergence Characteristics of the LMS Adaptive Filter for the Two-dimensional Array with Separable Weights in Estimating the Direction Cosine v at an Input SNR of 0 dB -----	86
27.	The RMS Error in Estimating the Direction Cosines u and v using the Two-dimensional Array with Separable Weights at an Input SNR of 0 dB -----	87
28.	The RMS Error in Estimating u and v Versus Input SNR -----	89
29.	System Geometry for the Homogeneous Medium Case ---	92
30.	System Geometry for the Inhomogeneous Medium Case -	93

31.	The RMS Error in Estimating u and v Versus Input SNR for the CW Pulse/Homogeneous Medium Case -----	101
32.	The RMS Error in Estimating u and v Versus Input SNR for the LFM Pulse/Homogeneous Medium Case -----	102
33.	The RMS Error in Estimating u and v Versus Input SNR for the CW Pulse/Inhomogeneous Medium Case -----	106
34.	The RMS Error in Estimating u and v Versus Input SNR for the LFM Pulse/Inhomogeneous Medium Case -----	108
35.	Different Ways of Adding Up Vectors to Obtain the Same Resultant -----	117
36.	Convergence Coefficient (Constant Value) Too Large -----	120
37.	Convergence Coefficient (Constant Value) Too Small -----	121
38.	Optimum Convergence Coefficient (Constant Value) --	122

## I. INTRODUCTION

Frequency domain beamforming is accomplished by applying appropriate phase shifts at the sensor outputs of an array to account for the relative propagation delays of a signal from a particular direction. The phase-shifted signals from all sensors are then added together coherently to realize the full array gain. Discrete Fourier Transform (DFT) beamforming is the usual method of determining the direction of arrival of a plane wave signal. A discrete number of spatial frequency bins are formed and each bin corresponds to a discrete direction. If the number of spatial frequency bins is large, very fine spatial resolution can be obtained.

The phase shifts needed to cancel the relative propagation delays can be determined adaptively. The complex LMS adaptive algorithm is used in this thesis. The LMS adaptive filter adjusts its adaptive weights recursively to minimize the mean square difference between a reference signal and its estimate. When the beam is steered toward a signal propagating in a particular direction, the phase of the signals at all sensors must be the same. Therefore, the signal at any sensor can be used as a reference which the others will be matched. The estimated signal is obtained by weighting the input signal by the current adaptive weights. Note that no prior knowledge of the reference signal is

required. The response of the LMS adaptive filter converges to the discrete Wiener filter without a priori knowledge of the input [Refs. 1,2]. [Ref. 1] proposed the complex LMS algorithm to deal with complex inputs. [Ref. 5] addressed the implementation of the LMS adaptive filter in the frequency domain. [Ref. 4] used the LMS adaptive filter in the frequency domain to estimate the bearing of a plane wave due to an acoustic source radiating a sinusoidal signal. In this application, the LMS adaptive filter was implemented to estimate the phase difference between two sonar arrays separated by a distance many times the signal wavelength. The angle of arrival of a plane wave can be estimated if the frequency of the acoustic signal and the speed of wave propagation are known or can be extracted from the received signal itself.

The objective of this thesis is to extend the results in [Ref. 3] and [Ref. 4] to a planar array of  $M \times N$  elements (hydrophones) where  $M$  and  $N$  are greater than two. Such an array has an overall size many times the wavelength of the received signal. The inter-element separation, however, is usually maintained at a distance of less than or equal to one-half of the expected minimum wavelength. This requirement [Ref. 5] prevents the occurrence of grating lobes in the far-field beam pattern. A two-dimensional array allows spatial resolution in both azimuth and elevation. Even though the detection range in underwater acoustics is large

compared to the ocean depth, the effect of ray bending due to the inhomogeneous ocean medium can bend the incident acoustic wave such that it can appear to arrive at a steeper or shallower angle than the line of sight angle in the homogeneous medium case. The elevation/depression angle is at present used to estimate Convergence Zone (CZ) and Bottom Bounce (BB) ranges.

In this thesis, the problem of a plane wave incident upon a planar array of  $M \times N$  elements is studied. The acoustic wave signal at each of the elements in the array are identical if the array is steered in the direction of the incident wavefront. However, if the main lobe of the array is not steered properly, the plane wave signal will have the same spectral content at each element but modified by a phase shift proportional to the location of the element with respect to some reference element. These undesirable phase shifts can be cancelled by applying appropriate phase weights at each element and thereby cophasing the total array output to realize its array gain. [Ref. 4] demonstrated that the LMS adaptive filter can achieve phase alignment between a reference signal and input signal in the frequency domain by direct application of the complex LMS algorithm. This is equivalent to a tapped delay line structure in the time domain. However, in the frequency domain, a time delay  $\tau$  corresponds to multiplication of a complex number that is equal to  $e^{j\omega\tau}$  where  $\omega$  is the signal frequency. The

implementation of the LMS adaptive filter in the frequency domain requires fewer computations per iteration than in the time domain. An added advantage of using phase weighting is that a continuous range of spatial directions can be described, whereas in a tapped delay line structure, only finite increments of delays can be applied. Figure 1 shows a functional diagram of an N-element adaptive array implemented in the frequency domain [Ref. 6].

Chapter II of this thesis describes the specific structure of the adaptive filter and the equations implemented for simulations. The assumptions made in the model are discussed and justified. Several modifications to the complex LMS adaptive algorithms are made to increase the array's spatial coverage and to ensure that the steady state phase weights do correspond to the direction of the incident wave.

In Chapter III, a passive sonar system is modeled to test the ability of the modified complex LMS algorithm to estimate the direction of a source in the presence of noise. The simulation program is implemented in VS APL.

Chapter IV demonstrates the application of the complex LMS algorithm to a pulse communication problem. The integration time in this case is much shorter than that of the passive sonar case. Two types of pulse waveforms are included, continuous wave (CW) and linear frequency-modulated (LFM). This simulation program is implemented in VS FORTRAN.

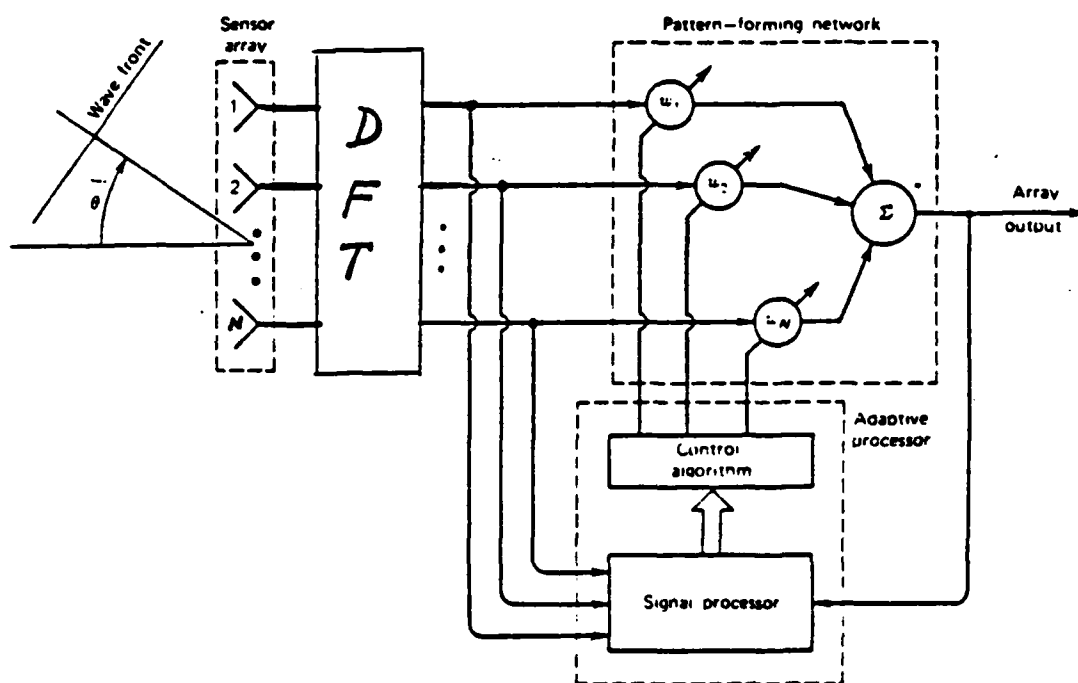


Figure 1. Frequency Domain Adaptive Array  
[Ref. 6:p. 7]

Chapter V concludes this thesis by identifying further research areas and other possible applications.

Appendix A contains the derivation of the complex LMS algorithm. Appendix B has the description of the passive detection program implemented in APL. Appendix C has the description of the pulse communication program implemented in VS Fortran.

## II. THEORY OF SYSTEM MODEL

### A. OVERVIEW OF ARRAYS [Refs. 5,6,7,8]

The characteristics of the array elements and their arrangement in forming the array determine the ultimate performance of an adaptive array system [Ref. 6]. Both the linear array and the planar array are examined here.

#### 1. Linear Arrays [Refs. 5,8]

Consider a linear array that has M equally spaced, identical point source elements along the x-axis. For illustration, Figure 2 shows a 7-element linear array with uniform interelement spacing  $d_x$  and a plane wave arriving at the array with an incident angle  $\theta$  as measured from the array normal. The phasor sum of all elements is:

$$s(t) = \sum_{m=0}^{M-1} y(t) e^{jm\psi} \quad (2.1)$$

where  $\psi$  is the phase shift between the  $m^{\text{th}}$  and the  $m+1^{\text{th}}$  element for  $m = 0, 1, 2, 3, \dots, M-1$ .

$$\psi = k \frac{d_x \sin \theta}{c} = \frac{2\pi}{\lambda} \left( \frac{d_x \sin \theta}{c} \right) \quad (2.2)$$

where:

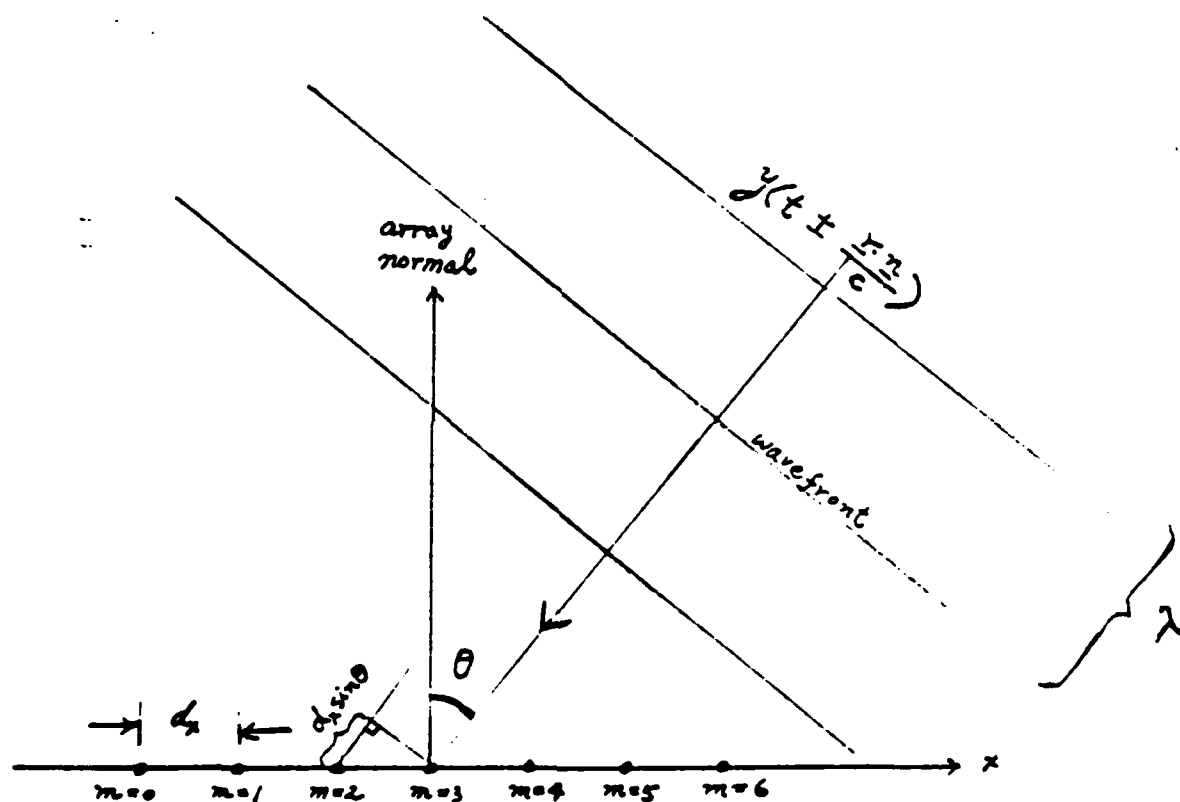


Figure 2. A Seven-Element Linear Array with Uniform Interelement Spacing and Point Source Elements

- $k$  = wave number in radians per meter
- $\lambda$  = wavelength in meters
- $f$  = frequency in hertz
- $d_X$  = interelement spacing in meters
- $\theta$  = incident angle measured from array normal
- $c$  = speed of wave propagation in meters per second.

Rewriting equation (2.2) by substituting  $\lambda = c/f$  yields

$$\psi = \frac{2\pi f}{c} \frac{d_X \sin \theta}{c} \quad (2.3)$$

The Fourier transform of equation (2.1) is:

$$S(f) = F\{s(t)\} = \int_{-\infty}^{\infty} s(t) e^{-j2\pi f t} dt \quad (2.4)$$

$$= \int_{-\infty}^{\infty} \sum_{m=0}^{M-1} y(t) e^{jm\psi} e^{-j2\pi f t} dt \quad (2.5)$$

$$= \sum_{m=0}^{M-1} e^{jm\psi} \int_{-\infty}^{\infty} y(t) e^{-j2\pi f t} dt \quad (2.6)$$

$$s(f, \theta) = A(f, \theta) Y(f) \quad (2.7)$$

where  $Y(f)$  is the frequency spectrum of the incident wave and  $A(f, \theta)$  is called the space factor or array factor. The array

factor  $A(f, \theta)$  determines the directional plane of the array in a plane containing the array. The dependence of  $A(f, \theta)$  on frequency, speed of propagation, element separation, number of elements, and incident angle can be shown by rewriting  $A(f, \theta)$  as:

$$A(f, \theta) = \sum_{m=0}^{M-1} e^{jm\psi} = \sum_{m=0}^{M-1} e^{jm \left( \frac{2\pi f}{c} d_X \sin \theta \right)} \quad (2.8)$$

Summing equation (2.8) yields:

$$A(f, \theta) = e^{j\frac{M}{2}\psi} \frac{\sin \frac{M}{2}\psi}{\sin \frac{\psi}{2}} \quad (2.9)$$

The normalized directional pattern is given by:

$$G(f, \theta) = 10 \log_{10} \left\{ \frac{|A(f, \theta)|^2}{M^2} \right\} \quad (2.10)$$

For nonisotropic (non-point source) elements, it is necessary to introduce an additional factor  $E(f, \theta)$  in equation (2.9) to include the directional response pattern introduced by each sensor element [Ref. 6]. The overall directivity pattern then is given by the produce of the array factor and the element factor [Ref. 5]. However, if the size of the individual

elements are small compared to a wavelength, they can be assumed to be omnidirectional point sources, i.e.,  $E(f, \theta) = 1$ . The effects of increasing the number of elements while maintaining the same element spacing are shown in Figures 3 and 4 [Ref. 6]. It can be seen that the main lobe beamwidth decreases as the number of elements increases, and the number of sidelobes and nulls increases. In Figures 5-8, the number of elements is held constant at  $M = 7$  while the interelement spacing is varied to illustrate the effects of elements spacing on the directivity pattern.

Beamsteering [Ref. 5] is accomplished by applying a linear phase shift across the line array as shown in Figure 9 [Ref. 6]. The effect of the insertion of this sequence of phase shifts is that the main lobe is steered to an angle as measured off the boresight equal to  $\theta$  where

$$\theta = \sin^{-1} \left\{ \frac{1}{2} \frac{\lambda}{d_x} \delta \right\} \quad (2.11)$$

and  $\delta$  is the phase shift between adjacent elements. Figure 10 shows the directivity pattern of a steered linear array.

## 2. Planar Arrays [Refs. 5,6]

Much of the analysis done in linear arrays can be extended to the case of a rectangular-shaped planar array. A circular planar array or a spherical volume array would require the use of polar and spherical coordinates respectively. However, array theory is invariant under coordinate transformations.

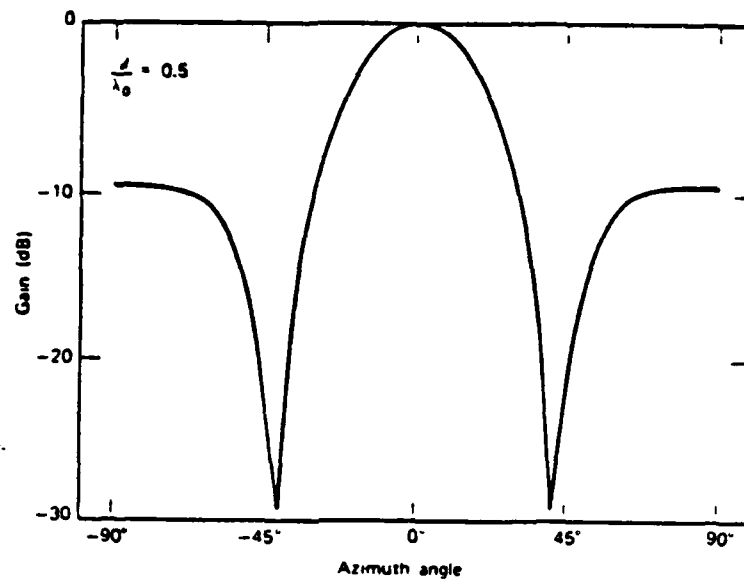


Figure 3. Directivity Pattern of a Three-Element Linear Array [Ref. 6:p. 40]

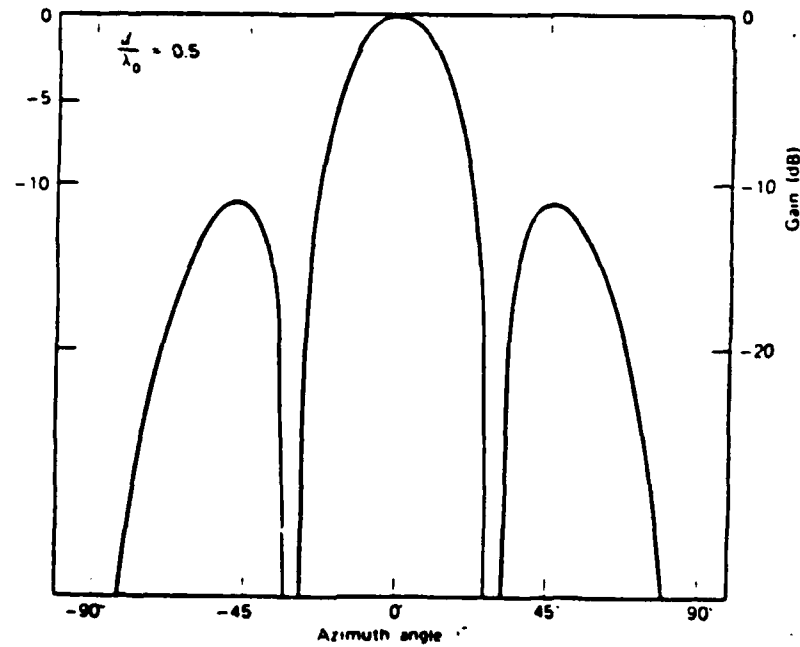


Figure 4. Directivity Pattern of a Four-Element Linear Array [Ref. 6:p. 40]

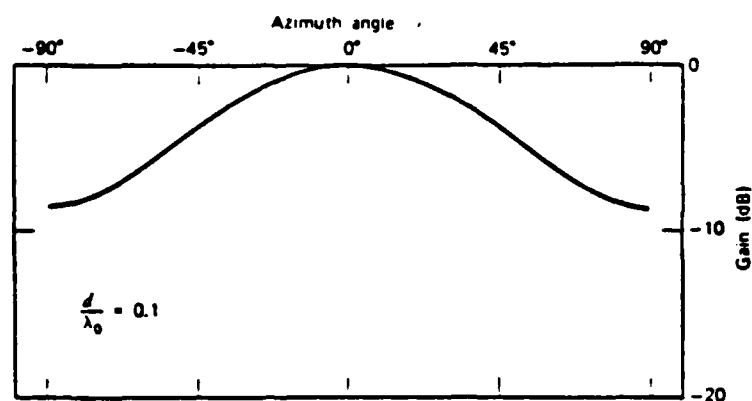


Figure 5. Directivity Pattern of a Seven-Element Linear Array for  $d/\lambda = 0.1$  [Ref. 6:p. 41]

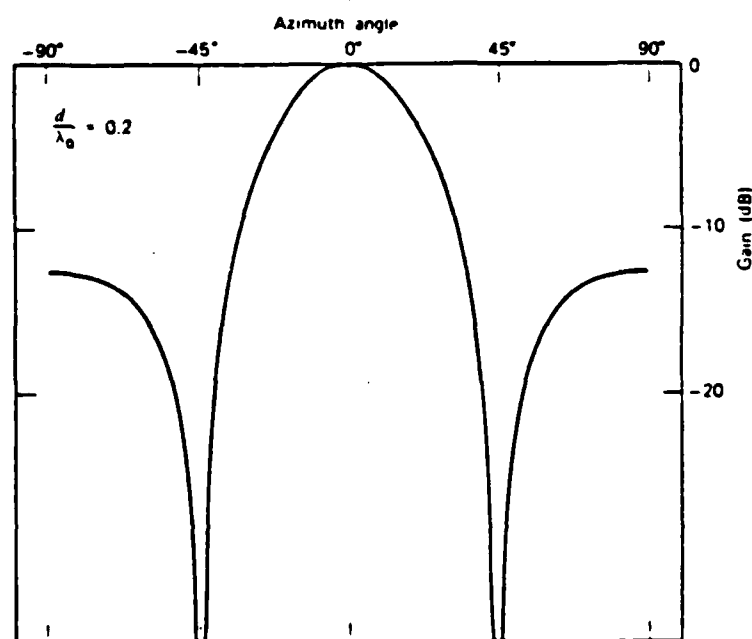


Figure 6. Directivity Pattern of a Seven-Element Linear Array for  $d/\lambda = 0.2$  [Ref. 6:p. 41]

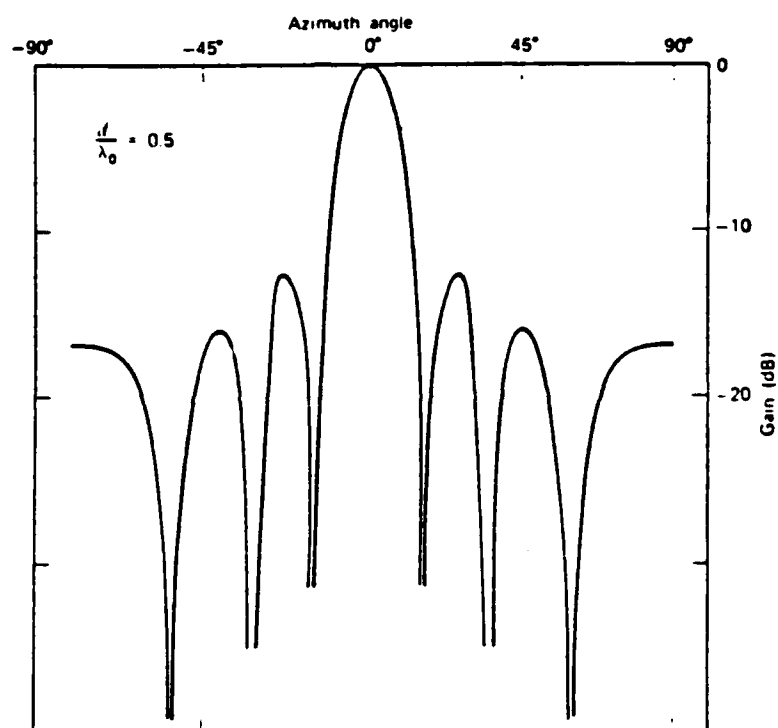


Figure 7. Directivity Pattern of a Seven-Element Linear Array for  $d/\lambda = 0.5$  [Ref. 6:p. 42]

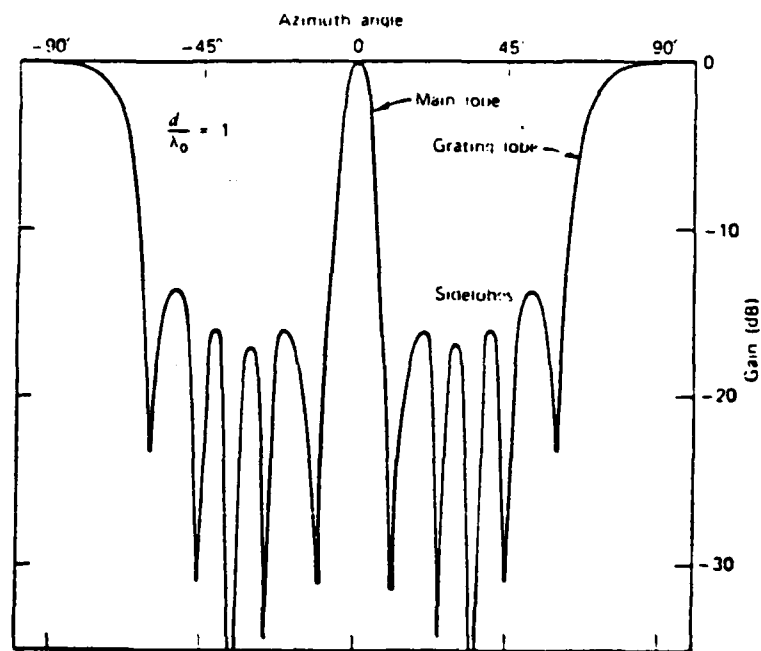


Figure 8. Directivity Pattern of a Seven-Element Linear Array for  $d = \lambda$  [Ref. 6:p. 42]

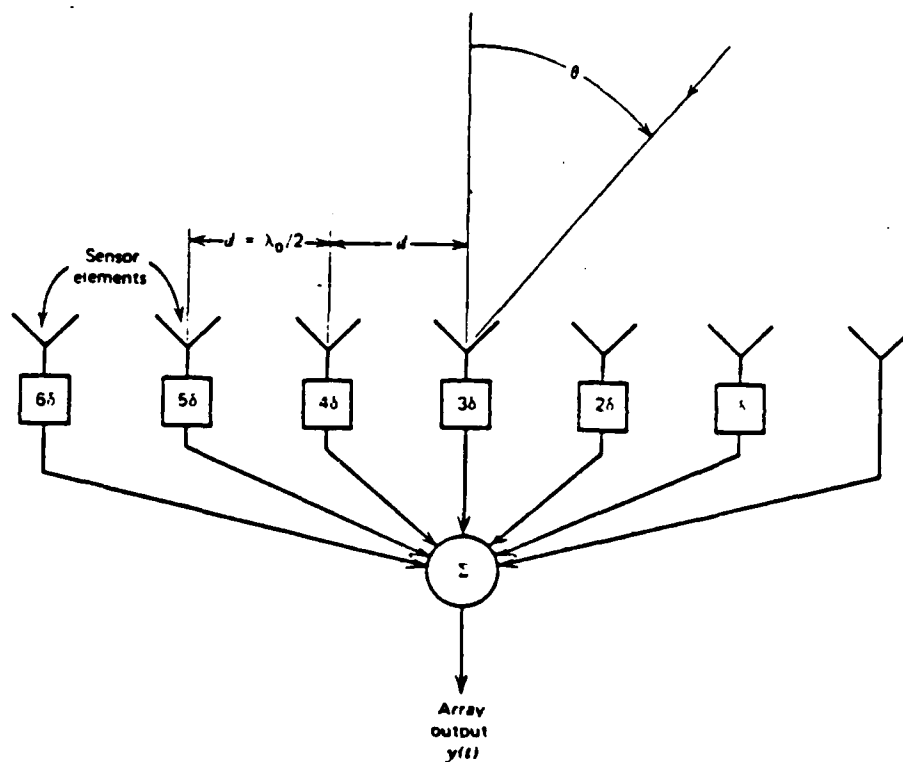


Figure 9. Beamsteering by Applying a Linear Phase Shift Across the Array [Ref. 6:p. 43]

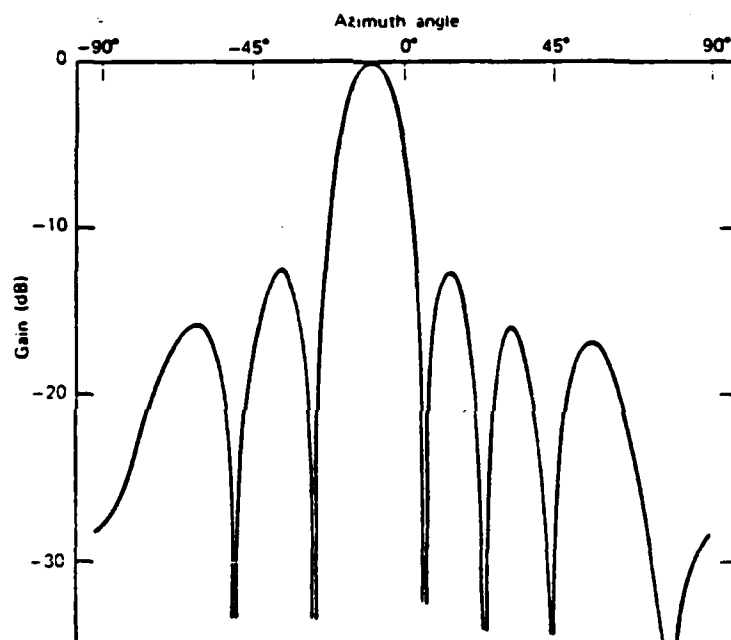


Figure 10. Steered Directivity Pattern [Ref. 6:p. 44]

A planar array has the advantage of resolving the azimuthal and the elevation angles of arrival of an incident plane wave [Refs. 5,9]. Consider a rectangular-shaped planar array as shown in Figure 11; sensor elements are arranged in a rectangular grid in the x-y plane. The center of the array is usually chosen as the coordinate origin. The entire array has M elements in the x-direction with uniform spacing  $d_x$  and N elements in the y-direction with uniform spacing  $d_y$ . The elements are assumed to be point sources. The phasor sum of the entire array can be written as:

$$s(t) = \sum_m \sum_n y(t) e^{jm\psi_x} e^{jn\psi_y} \quad (2.12)$$

where

$$\psi_x = 2\pi \left( \frac{d_x}{\lambda} \right) \sin \theta \cos \phi \quad (2.13)$$

$$\psi_y = 2\pi \left( \frac{d_y}{\lambda} \right) \sin \theta \sin \phi \quad (2.14)$$

The directivity pattern of the planar array is given by:

$$A(f, \theta, \phi) = \sum_m \sum_n e^{jm\psi_x} e^{jn\psi_y} = A_x(f, \theta, \phi) A_y(f, \theta, \phi) \quad (2.15)$$

It follows from the model given by equation (2.12) that the planar array beam pattern is the product of the array factors

of two linear arrays. However, separability of the two-dimensional beam pattern is not necessary to ensure the proper operation of the LMS adaptive algorithm for a planar array. Beamsteering is accomplished by applying appropriate linear phase shifts for the row and column elements. For the rectangular array case under investigation here, it is more convenient to transform the elevation-azimuth  $(\theta, \phi)$  space to a rectilinear coordinate space  $(u, v)$  by the transformation:

$$u = \sin \theta \cos \phi \quad (2.16)$$

$$v = \sin \theta \sin \phi \quad (2.17)$$

The parameters  $u$  and  $v$  are the direction cosines with respect to the  $x$  and  $y$  axes, respectively. Figure 12 shows the alternate diagrams for presenting two-dimensional array beam patterns [Ref. 6]. The ranges of the spherical angles are  $0 \leq \theta \leq \pi/2$  and  $0 \leq \phi \leq 2\pi$  whereas the ranges of the rectilinear coordinate system are  $-1 \leq u \leq 1$  and  $-1 \leq v \leq 1$ .

## B. THE PLANE WAVE MODEL

### 1. Far-Field Condition

The LMS adaptive filter designed in this thesis will provide spatial resolution for a planar array for an incident plane-wave field. The plane wave assumption is justifiable for a radiating source located in the far-field

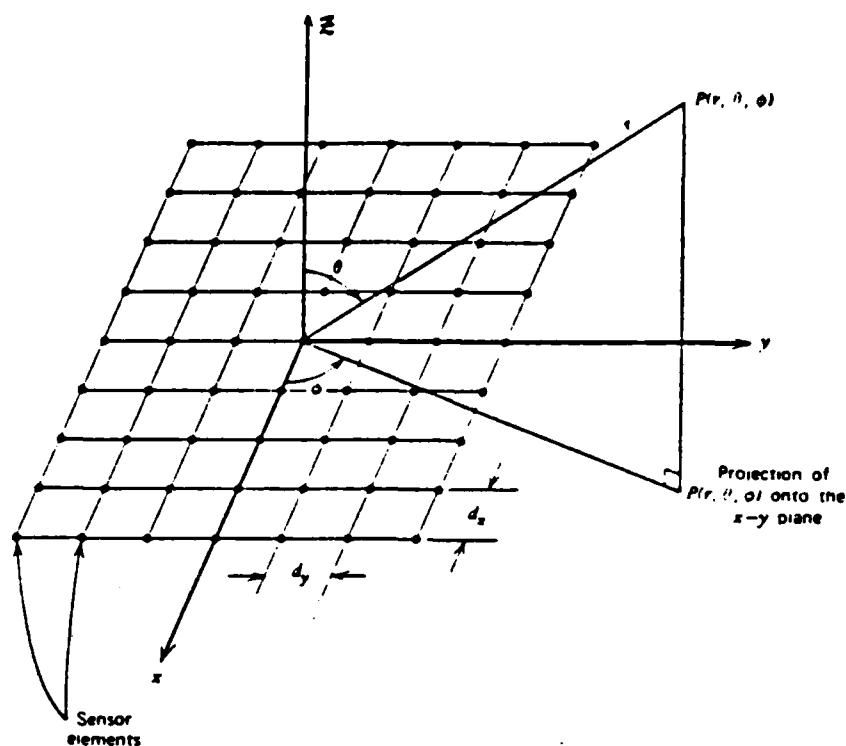


Figure 11. Sensor Element Arrangement of a Rectangular Planar Array [Ref. 6:p. 45]

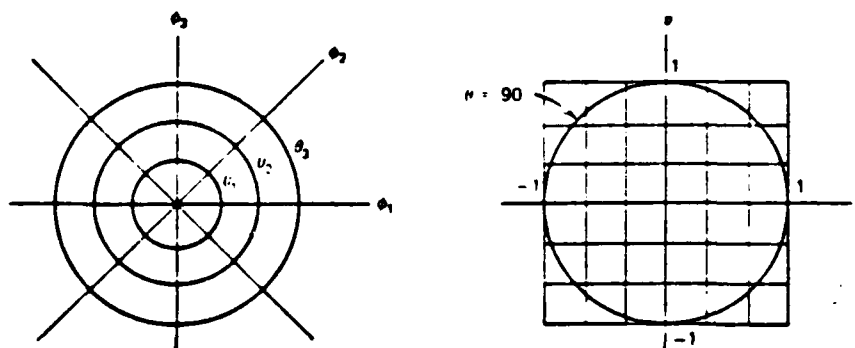


Figure 12. Transformation from Spherical Coordinate Space to Direction Cosine Space [Ref. 6:p. 46]

[Refs. 5,10], due to wavefront expansion. The far-field range for a planar array is given by [Ref. 5]:

$$R > \frac{\pi D^2}{\lambda} \quad (2.18)$$

where:

$$D = \left\{ \left( \frac{L_x}{2} \right)^2 + \left( \frac{L_y}{2} \right)^2 \right\}^{1/2} \quad (2.19)$$

represents the maximum radial extent of the transducer array and  $L_x$  and  $L_y$  are the dimensions of the planar array in the  $x$  and  $y$  directions, respectively.

## 2. Propagation of a Plane Wave from a Far-Field Source

The plane wave solution of the Helmholtz wave equation has the form:

$$y(t, \underline{r}) = Ae^{j(2\pi ft + \underline{k} \cdot \underline{r})} \quad (2.20)$$

where  $y(t, \underline{r})$  is called the velocity potential,  $f$  is the frequency,  $\underline{k}$  is the propagation vector, and  $\underline{r}$  the position vector. In rectangular coordinates,

$$\underline{k} = k_x \hat{x} + k_y \hat{y} + k_z \hat{z} \quad (2.21)$$

and

$$\underline{r} = x \hat{x} + y \hat{y} + z \hat{z} \quad (2.22)$$

For a planar array located at some reference location  $z = 0$ , the velocity potential is:

$$y(t, \underline{r}) = y(t, x, y) = Ae^{j[2\pi ft + (k_x x + k_y y)]} \quad (2.24)$$

For a planar array with discrete sensor elements located uniformly in the  $x$ - $y$  plane with spacings  $d_x$  and  $d_y$  respectively, the continuous space variable  $x$  can be replaced by  $md_x$  and  $y$  replaced by  $nd_y$ . If the time signal is digitized for computer processing, then the time variable  $t$  can be replaced by  $\ell T_s$ , where  $\ell$  is the discrete time index and  $T_s$  the sampling interval. To summarize:

$$t \rightarrow \ell T_s \quad (2.25a)$$

$$x \rightarrow md_x \quad (2.25b)$$

$$y \rightarrow nd_y \quad (2.25c)$$

The corresponding discrete time, sampled space signal is given by:

$$y(\ell T_s, md_x, nd_y) = Ae^{j2\pi f\ell T_s} e^{j(md_x k_x + nd_y k_y)} \quad (2.26)$$

where  $y(\ell T_s, md_x, nd_y)$  is usually shorted to  $y(\ell, m, n)$ . The propagation vector  $\underline{k}$  at  $z = 0$  has two components  $k_x$  and  $k_y$

that can be related to the direction cosines  $u$  and  $v$  via [Ref. 5]:

$$k_x = \frac{2\pi u}{\lambda} \quad (2.27a)$$

and

$$k_y = \frac{2\pi v}{\lambda} \quad (2.27b)$$

Substituting equation (2.27) into equation (2.26) yields:

$$y(\ell, m, n) = Ae^{j2\pi f \ell T_s} e^{j\frac{2\pi}{\lambda}(um d_x + vnd_y)} \quad (2.28)$$

Let

$$y(\ell) = Ae^{j2\pi f \ell T_s} \quad (2.29)$$

represent the time dependence of the signal. Equation (2.28) then becomes:

$$y(\ell, m, n) = y(\ell) e^{j\frac{2\pi}{\lambda}(um d_x + vnd_y)} \quad (2.30)$$

From equation (2.30), it is easy to see that the signal at each element location  $(m, n)$  has the same time dependence but has a different phase due to the element location and

the direction cosines associated with the incident angle of the plane wave upon the array. The exponential relationship of the phase in equation (2.30) also suggests that the phases in the x and y directions are separable.

### C. FREQUENCY DOMAIN LMS ADAPTIVE FILTER FOR SPATIAL RESOLUTION

The objective of the LMS adaptive filter used in this thesis is to phase align the signals from all sensor elements such that they add up coherently to realize the full array gain. Figure 13 shows a general cophasing scheme for linear arrays. Cophasing or phase alignment is done in the frequency domain by multiplying the frequency spectrum at each element by the proper phase weight in order to cancel out the phase due to element location. This is equivalent to a phasor rotation in the complex plane. The amount of rotation needed to align each sensor element is proportional to the frequency of interest, the direction cosines  $u$ ,  $v$  and the location of that element.

#### 1. Phase Weights for the Planar Array

The total array output is maximized if all elements in the array are phase aligned. If we let  $cd(m,n)$  be the proper phase weight at location  $(m,n)$ , then the phase weighted total array output is:

$$s(l) = \sum_m \sum_n cd(m,n) y(l,m,n) \quad (2.31)$$

Substituting equation (2.30) into equation (2.31) gives:

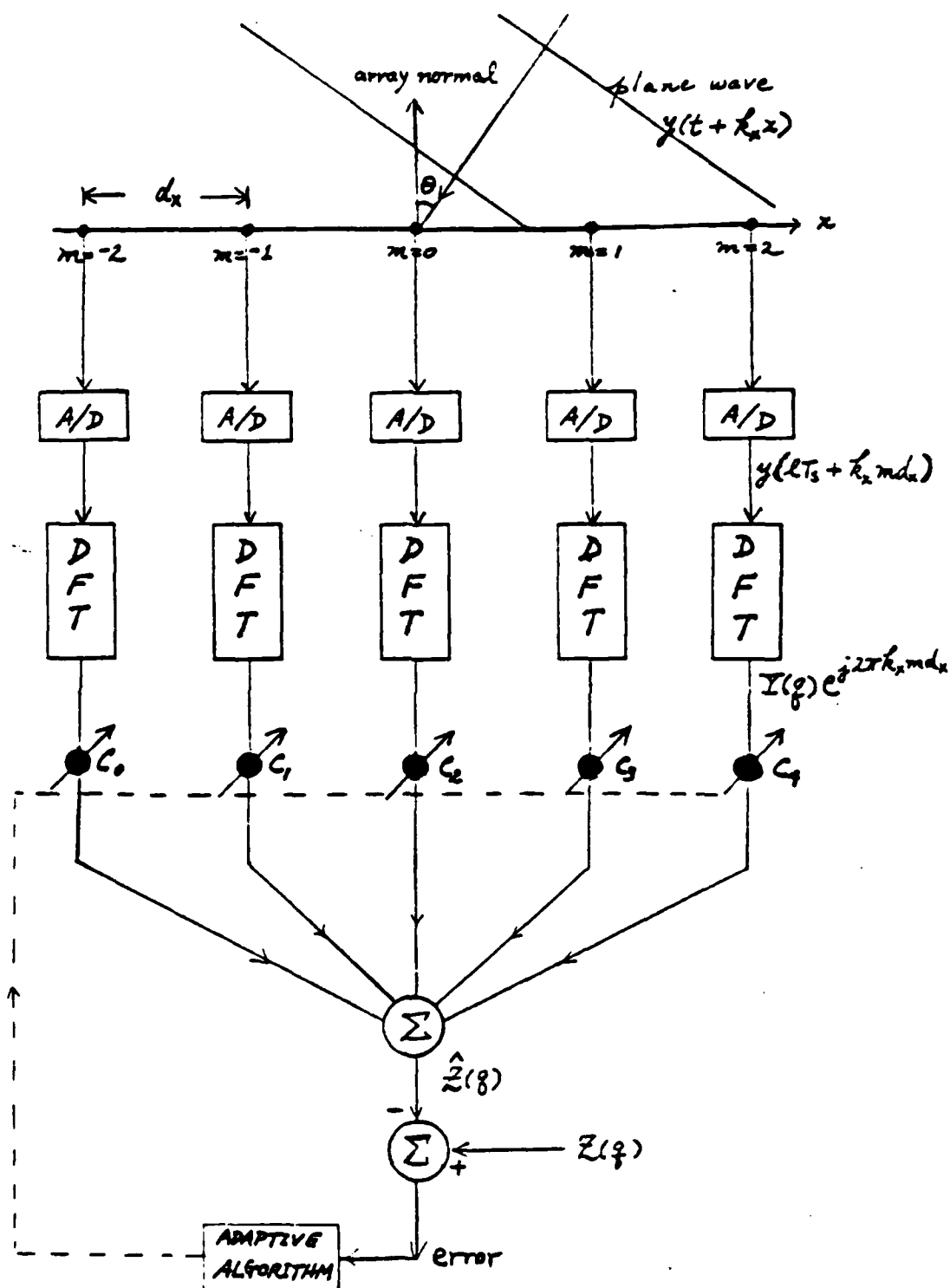


Figure 13. Adaptive Cophasing Scheme for a Linear Array

$$s(\ell) = y(\ell) \sum_m \sum_n cd(m,n) e^{j \frac{2\pi}{\lambda} (umd_X + vnd_Y)} \quad (2.32)$$

If

$$cd(m,n) = e^{-j \frac{2\pi}{\lambda} (umd_X + vnd_Y)} \quad (2.33)$$

then the quantity inside the summations becomes unity and:

$$s(\ell) = y(\ell) \sum_m \sum_n (1) \quad (2.34)$$

or

$$s(\ell) = MN y(\ell) \quad (2.35)$$

where  $s(\ell)$  is the sum over all elements and equation (2.35) is the maximum signal level possible. This maximum level is achieved by tuning  $M \times N$  adaptive weights  $cd(m,n)$  to conform to equation (2.33). The same phase weighting procedure is also true in the frequency domain, in fact, the implementation of phase weighting is inherently a frequency domain operation. Since phase weight equation (2.33) is a function of wavelength  $\lambda$  and  $\lambda = c/f$ , the proper phase weight for co-phasing at each element is a function of frequency  $f$ . Thus for each valid frequency component in the signal, a different

set of phase weights  $\{cd(m,n)\}$  must be generated. Consider the DFT with respect to time of equation (2.32):

$$S(q) = Y(q) \sum_m \sum_n cd(m,n) e^{j\frac{2\pi}{\lambda}(umd_x + vnd_y)} \quad (2.36)$$

where  $q$  is the frequency index and  $Y(q)$  is the DFT of  $y(\ell)$ .

If equation (2.33) holds, then:

$$S(q) = Y(q) \sum_m \sum_n (1) = MN Y(q) \quad (2.37)$$

Only valid spectral lines will be processed.

## 2. The Frequency Domain LMS Adaptive Filter

The general frequency domain LMS adaptive algorithm is derived in Appendix A. Suppose that the time signal  $z(\ell)$  is the reference or desired signal and  $\hat{z}_i(\ell)$  is the normalized sum of all signals in the planar array. In the frequency domain, the reference signal in the  $q^{\text{th}}$  DFT bin is:

$$Z(q) = \sum_{\ell=0}^{L-1} z(\ell) e^{-j\frac{2\pi}{L}\ell q} \quad (2.38)$$

and the estimated output in the frequency domain is:

$$\hat{Z}_i(q) = \sum_{\ell=0}^{L-1} \hat{z}_i(\ell) e^{-j\frac{2\pi}{L}\ell q} \quad (2.39)$$

Substituting equation (2.31) with  $\hat{z}_i(\ell) = \frac{1}{MN} s_i(\ell)$  yields:

$$\hat{z}_i(q) = \sum_{\ell=0}^{L-1} \frac{1}{MN} \sum_m \sum_n c d_i(m,n) y(\ell,m,n) e^{-j \frac{2\pi}{L} \ell q} \quad (2.40)$$

where:

$\ell$  is the time index;  $\ell = 0, 1, \dots, L-1$

$q$  is the DFT bin index;  $q = 0, 1, \dots, Q-1$

$i$  is the complex phase weight iteration number.

The DFT operation with respect to time in equation (2.40) can be performed first to yield:

$$\hat{z}_i(q) = \frac{1}{MN} \sum_m \sum_n c d_i(m,n) Y(q,m,n) \quad (2.41)$$

where:

$$Y(q,m,n) = \sum_{\ell=0}^{L-1} y(\ell,m,n) e^{-j \frac{2\pi}{L} \ell q} \quad (2.42)$$

Based on the complex LMS algorithm [Ref. 1], the adaptive filter output in the  $q^{\text{th}}$  bin is given by equation (2.41).

The error signal is generated by comparing the desired (reference) signal to the adaptive filter output (estimate).

The error is denoted by  $e_i$ , where:

$$e_i = z(q) - \hat{z}_i(q) \quad (2.43)$$

The estimate, equation (2.41), is formed by applying the phase weights  $\{cd_i(m,n)\}$  of the  $i^{\text{th}}$  iteration to each element in the planar array. The complex weight  $cd_i(m,n)$  is updated recursively as follows:

$$cd_{i+1}(m,n) = cd_i(m,n) + 2\mu_i e_i y^*(q,m,n) \quad (2.44)$$

where:

$$m = 0, 1, \dots, M-1$$

$$n = 0, 1, \dots, N-1$$

(\*) denotes complex conjugate

$\mu_i$  = feedback coefficient, a parameter that controls the rate of convergence, algorithm noise, and the stability of the algorithm [Ref. 4].

From equation (2.44), it can be seen that the  $i+1^{\text{th}}$  weight  $cd_{i+1}(m,n)$  may have magnitudes larger than unity. This growth in magnitude is undesirable for the purpose of spatial resolution since spatial resolution depends on the relative phase between adjacent elements to resolve the direction of wave arrival. Thus, a normalization is necessary to bring equation (2.44) back to unity. This normalization is:

$$cd_{i+1}(m,n) \leftarrow cd_{i+1}(m,n) / |cd_{i+1}(m,n)| \quad (2.45)$$

These updated and normalized phase weights can now be applied to equations (2.41), (2.43), and (2.44) in sequence to compute the next set of phase weights. This iterative process stops when predetermined criteria are met. At that point, the set of phase weights  $\{cd_i(m,n)\}$  can be used to find the direction cosines of the incident plane wave. However, the phase angles of the phase weights  $\{cd_i(m,n)\}$  may have been wrapped around an integer multiple of  $2\pi$ . The procedure for phase unwrapping is explained in Sections 4 and 5 of this chapter.

The feedback coefficient  $\mu_i$  in equation (2.44) controls the rate of convergence and the stability of the LMS adaptive filter. Robbins and Monro [Ref. 11] showed that the adaptive weights  $\{cd_i(m,n)\}$  will converge to the optimum result if  $\mu_i$  is allowed to decrease with the iteration index  $i$ . The precise conditions are [Ref. 12]:

$$\mu_i > 0$$

$$\lim_{i \rightarrow \infty} \mu_i = 0$$

$$\sum_{i=1}^{\infty} \mu_i = \infty$$

$$\sum_{i=1}^{\infty} \mu_i^2 < \infty$$

A coefficient  $\mu_i$  that satisfies the above conditions will work as long as the signal and noise inputs are truly stationary but will not be satisfactory for a filter operating in a slowly varying environment. Widrow's LMS algorithm [Ref. 1] uses a constant value of  $\mu$  satisfying the inequality

$$0 < \mu < \lambda_{\max}^{-1}$$

where  $\lambda_{\max}$  is the largest eigenvalue of the correlation matrix of the input. Although this matrix is typically not known a priori, some bound can be set up by examining equation (2.44). If stationarity can be assumed, it is possible to update  $\mu_i$  every iteration in order to obtain the optimum set of phase weights. In Appendix A a simple method of updating the feedback coefficient  $\mu_i$  is proposed to improve the performance of the LMS adaptive filter.

### 3. Applying the Frequency Domain LMS Adaptive Filter to a Planar Array

Given a rectangular planar array with  $M \times N$  elements, there are several ways to process the signal from the array to achieve spatial resolution in both azimuth and elevation. Three different ways are considered in this thesis.

### a. Orthogonal Linear Arrays

Two-dimensional spatial resolution is possible by just considering one linear array in the x-direction and one linear array in the y-direction. A total of  $M+N-1$  elements out of  $M \times N$  are used. This scheme is useful when processing time is limited. Figure 14 illustrates the choice of the center linear arrays for this scheme. However, any two orthogonal linear arrays in the planar array can be used. The recursive equations needed to implement this algorithm are divided into two sets; one set for the linear array in the x-direction and the other for the y-direction. In the x-direction the estimate is:

$$\hat{z}_{x_i}(q) = \frac{1}{M} \sum_{m=0}^{M-1} c_i(m) Y(q, m, n = n_0) \quad (2.46)$$

where:

$n_0$  = constant y-direction index

$c_i(m)$  = unity magnitude phase weight.

The error is the difference between the reference and the estimate.

$$e_{x_i} = z(q) - \hat{z}_{x_i}(q) \quad (2.47)$$

The recursive update for phase weights is:

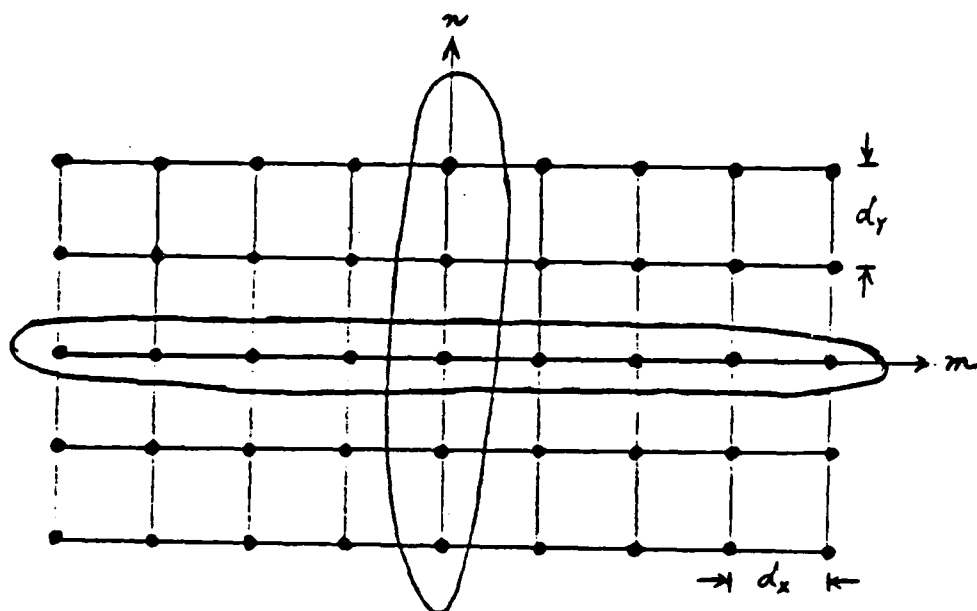


Figure 14. A Particular Orthogonal Linear Arrays Configuration

$$c_{i+1}(m) = c_i(m) + 2\mu_{x_i} e_{x_i} Y^*(q, m, n = n_0) \quad (2.48)$$

The phase of the new update is:

$$c_{i+1}(m) \leftarrow c_{i+1}(m) / |c_{i+1}(m)| \quad (2.49)$$

In the y-direction, the procedure is similar:

$$\text{Estimate: } z_{y_i}(q) = \frac{1}{N} \sum_{n=0}^{N-1} d_i(n) Y(q, m = m_0, n) \quad (2.50)$$

$$\text{Error: } e_{y_i} = z(z) - \hat{z}_{y_i}(q) \quad (2.51)$$

$$\text{Update: } d_{i+1}(n) = d_i(n) + 2\mu_{y_i} e_{y_i} Y^*(q, m = m_0, n) \quad (2.52)$$

$$\text{Normalization: } d_{i+1}(n) \leftarrow d_{i+1}(n) / |d_{i+1}(n)| \quad (2.53)$$

The convergence constants  $\mu_x$  and  $\mu_y$  are usually set to be equal since the statistics in the orthogonal directions of a planar array can be assumed to be the same for the observation time of most systems.

#### b. Two-dimensional Array

This scheme uses all  $M \times N$  elements and therefore it can realize the full array gain of equation (2.35). The

phase weights  $cd(m,n)$  are not assumed to be separable. The equations for the LMS adaptive filter in the frequency domain are:

$$\text{Estimate: } \hat{z}_i(q) = \frac{1}{MN} \sum_m \sum_n cd_i(m,n) Y(q,m,n) \quad (2.54)$$

$$\text{Error: } e_i = z(q) - \hat{z}_i(q) \quad (2.55)$$

$$\text{Update: } cd_{i+1}(m,n) = cd_i(m,n) + 2\mu_i e_i Y^*(q,m,n) \quad (2.56)$$

$$\text{Normalization: } cd_{i+1}(m,n) \leftarrow cd_{i+1}(m,n) / |cd_{i+1}(m,n)| \quad (2.57)$$

### c. Separable Two-dimensional Array

As mentioned in the discussion on planar arrays and plane waves, the form of a plane wave suggests that the phase of a signal at an element  $(m,n)$  is separable. This scheme then uses the separability property

$$cd(m,n) = c(m)d(n) \quad (2.58)$$

to implement a two-dimensional LMS adaptive filter. All  $M \times N$  elements are used but only  $M+N$  phase weights need to be updated recursively. The equations are:

$$\text{Estimate: } \hat{z}_i(q) = \frac{1}{MN} \sum_n d_i(n) \sum_m c_i(m) Y(q,m,n) \quad (2.59)$$

$$\text{Error: } e_i = Z(q) - \hat{Z}_i(q) \quad (2.60)$$

$$\text{Updates: } c_{i+1}(m) = c_i(m) + 2\mu_i e_i \left( \sum_n d_i(n) Y(q, m, n) \right)^* \quad (2.61)$$

$$d_{i+1}(n) = d_i(n) + 2\mu_i e_i \left( \sum_m c_i(m) Y(q, m, n) \right)^* \quad (2.62)$$

$$\text{Normalizations: } c_{i+1}(m) \leftarrow c_{i+1}(m) / |c_{i+1}(m)| \quad (2.63)$$

$$d_{i+1}(n) \leftarrow d_{i+1}(n) / |d_{i+1}(n)| \quad (2.64)$$

All three of the aforementioned schemes are implemented and their results compared. At the start of all three algorithms, the initial phase weights are set to the boresight of the planar array, i.e., magnitude equal to unity and phase angle to zero. The normalization of phase weights to unity forces the spatial transfer function of the LMS adaptive filter to have unit magnitude. The steady state phase response is designed to phase align all sensor elements in an element-by-element fashion. More discussion on this topic can be found in Appendix A.

#### 4. Extracting Estimates of the Direction Cosines $\hat{u}$ and $\hat{v}$ from Phase Weights

To extract  $\hat{u}$  and  $\hat{v}$  from the orthogonal linear arrays and the separable two-dimensional array cases discussed in Section C.3.a. and C.3.a.c., only  $M$  elements in the  $x$ -direction and  $N$  elements in the  $y$ -direction need to be considered.

a. Direction Cosine Estimates for Linear Arrays

Consider that in cases 3a. and 3c., the phase weights  $c(m)$ ,  $d(n)$  have reached a steady state. The objective at this point is to relate the phase angles of these two sets of phase weights to their respective direction cosines. Let  $\xi_x(m)$  be the phase angle of  $c(m)$  and  $\xi_y(n)$  be the phase angle of  $d(n)$ , i.e.,

$$\xi_x(m) = \tan^{-1} \left\{ \frac{\text{Im}[c(m)]}{\text{Re}[c(m)]} \right\} \quad (2.65a)$$

and

$$\xi_y(n) = \tan^{-1} \left\{ \frac{\text{Im}[d(n)]}{\text{Re}[d(n)]} \right\} \quad (2.65b)$$

It can be seen from equation (2.33) and using the concept of separability that:

$$\xi_x(m) = - \frac{2\pi}{\lambda} (\hat{u} m d_x) \quad (2.66a)$$

$$\xi_y(n) = - \frac{2\pi}{\lambda} (\hat{v} n d_y) \quad (2.66b)$$

Solving equation (2.66) for  $\hat{u}$  and  $\hat{v}$  yields:

$$\hat{u} = \frac{-\lambda \xi_x(m)}{2\pi m d_x}, \quad m \neq 0 \quad (2.67a)$$

$$\hat{v} = \frac{-\lambda \xi_y(n)}{2\pi n d_y}, \quad n \neq 0 \quad (2.67b)$$

Thus, in the x-direction, there are M-1 estimates of  $\hat{u}$ ; while in the y-direction, there are N-1 estimates of  $\hat{v}$ . To find an estimate of the direction cosines from equation (2.67), one needs to take an arithmetic average of possible estimates:

$$\hat{u} = \frac{1}{M-1} \sum_{m=1}^{M-1} \frac{-\lambda \xi_x(m)}{2\pi m d_x} \quad (2.68a)$$

$$\hat{v} = \frac{1}{N-1} \sum_{n=1}^{N-1} \frac{-\lambda \xi_y(n)}{2\pi n d_y} \quad (2.68b)$$

Equations (2.68a) and (2.68b) will be referred to as the point by point method. Another way of finding  $\hat{u}$  and  $\hat{v}$  makes use of linear regression [Ref. 13]. Consider equation (2.66) where  $\xi_x(m)$  is a linear function of m with slope equal to  $-\frac{2\pi\hat{u}}{\lambda}d_x$  and  $\xi_y(n)$  is a linear function of n with slope equal to  $-\frac{2\pi\hat{v}}{\lambda}d_y$ . Using a linear regression fit of M data points vs. the element number m, the slope and intercept of the line  $\xi_x(m)$  can be calculated. The same procedure can be used for  $\xi_y(n)$ . Let the slope in the x-direction be  $s_1$  and the slope in the y-direction be  $s_2$ . Then:

$$s_1 = -\frac{2\pi}{\lambda} \hat{u} d_x \quad (2.69a)$$

$$s_2 = -\frac{2\pi}{\lambda} \hat{v} d_y \quad (2.69b)$$

Thus,  $\hat{u}$  and  $\hat{v}$  can be solved by rearranging equation (2.69) to the form:

$$\hat{u} = \frac{-\lambda s_1}{2\pi d_x} \quad (2.70a)$$

$$\hat{v} = \frac{-\lambda s_2}{2\pi d_y} \quad (2.70b)$$

The estimates  $\hat{u}$  and  $\hat{v}$  obtained from the linear regression method represent the best linear least-squares fit of the observed data.

#### b. Direction Cosine Estimates for Planar Arrays

The two-dimensional array discussed in Section 3.b of this chapter does not require the phase weights to be separable. Consider that the set of phase weights  $\{cd(m,n)\}$  has reached a steady state. Let  $\xi_{xy}(m,n)$  be the phase angle associated with the  $cd(m,n)$ . Then:

$$\xi_{xy}(m,n) = \tan^{-1} \left\{ \frac{\text{Im}[cd(m,n)]}{\text{Re}[cd(m,n)]} \right\} \quad (2.71)$$

From equation (2.33), it can be seen that

$$\xi_{xy}(m,n) = - \frac{2\pi}{\lambda} (\hat{u} m d_x + \hat{v} n d_y) \quad (2.72)$$

In general,  $\xi_{xy}(m,n)$  can be a more complicated function of  $m$  and  $n$ . For instance, in the near-field problem, one needs to

modify equation (2.72) to contain quadratic phase terms to account for wavefront curvature [Ref. 5]. For the plane wave model, equation (2.72) adequately describes the phase weights needed to steer the directivity pattern of the planar array to the direction corresponding to  $\hat{u}$  and  $\hat{v}$ .

The point by point method is applicable here to find  $\hat{u}$  and  $\hat{v}$  given a steady state phase angle. However, a linear regression fit of  $\xi_{xy}(m,n)$  vs. the element index  $m$  and  $n$  appears to be more suited to this problem. Rewriting equation (2.72) in the form of the equation for a plane in three-dimensional space yields:

$$\xi_{xy}(m,n) = \left(\frac{-2\pi}{\lambda} \hat{u} d_X\right)m + \left(\frac{-2\pi}{\lambda} \hat{v} d_Y\right)n \quad (2.73)$$

Equation (2.73) describes a plane with slope  $-\frac{2\pi}{\lambda} \hat{u} d_X$  in the  $m$ -direction ( $x$ -direction) and slope  $-\frac{2\pi}{\lambda} \hat{v} d_Y$  in the  $n$ -direction ( $y$ -direction). Again, let the slopes be:

$$s_1 = -\frac{2\pi}{\lambda} \hat{u} d_X \quad (2.74a)$$

$$s_2 = -\frac{2\pi}{\lambda} \hat{v} d_Y \quad (2.74b)$$

Thus, equation (2.74) is identical to equation (2.70) and the direction cosine estimates  $\hat{u}$  and  $\hat{v}$  are found by equation (2.71), i.e.,

$$\hat{u} = \frac{-\lambda s_1}{2\pi d_x} \quad (2.71a)$$

$$\hat{v} = \frac{-\lambda s_2}{2\pi d_y} \quad (2.71b)$$

This result is not surprising since the exponential representation of the plane wave, equation (2.20), is inherently separable.

## 5. Unwrapping the Steering Phase Weights

### a. Linear Array Unwrapping

The proper phase weights for beamsteering are given by equation (2.66):

$$\xi_x(m) = \frac{-2\pi}{\lambda}(\hat{u} m d_x) \quad (2.66a)$$

$$\xi_y(n) = \frac{-2\pi}{\lambda}(\hat{v} n d_y) \quad (2.66b)$$

Consider a 7-element linear array lying in the x-direction with the center element as the reference element. The element index then runs from  $m = -3, -2, -1, 0, 1, 2, 3$ . If  $\hat{u}$  is equal to 0.55 and  $d_x = \lambda/2$ , then equation (2.67a) reduces to:

$$\begin{aligned} \xi_x(m) &= -\pi \hat{u} m \\ &= -0.55 \pi m \end{aligned} \quad (2.75)$$

The following table shows the required phase weights  $\xi_x(m)$  needed to steer the beam to  $\hat{u} = 0.55$ .

TABLE 1  
PHASE WEIGHTS FOR BEAMSTEERING

m	-3	-2	-1	0	1	2	3
$\xi_x(m)$	$1.65\pi$	$1.1\pi$	$.55\pi$	0	$-.55\pi$	$-1.1\pi$	$-1.65\pi$
$\xi'_x(m)$	$-.35\pi$	$-.9\pi$	$.55\pi$	0	$-.55\pi$	$0.9\pi$	$.35\pi$

The phase factors  $\{e^{j\xi_x(m)}\}$  are a set of complex numbers in the complex plane. The angle of any complex number must lie within a  $2\pi$  interval. The interval chosen here is  $[-\pi, \pi]$ . This means that any angle  $\xi_x(m)$  that is outside the range  $[-\pi, \pi]$  will be wrapped around to an angle  $\xi'_x(m)$  that is inside the range. This property can be shown as follows:

$$e^{j(\beta+2\pi k)} = e^{j\beta} e^{j2\pi k} = e^{j\beta} \quad (2.76)$$

since

$$e^{j2\pi k} = 1 \quad \text{for } k = 0, \pm 1, \pm 2, \dots$$

therefore

$$e^{j\beta} \text{ has modulo } 2\pi.$$

Referring back to Table 1, the observed angles  $\xi'_x(m)$  are wrapped. If no processing is done to unwrap the observed angles, the equations derived in Section C.4 of this chapter will not apply for all permissible values of  $\hat{u}$  and  $\hat{v}$ . For small values of  $\hat{u}$  or  $\hat{v}$ , the needed phase weights do not wrap around but the spatial range of interest is severely restricted [Ref. 4]. In tracking systems, the above restriction in look direction can be justified since a crude target direction is usually provided by a search array. The maximum spatial window of an M element linear array without the unwrapping of the steering phase weights can be calculated. For example, given that the element spacing is  $d_x = \lambda/2$ , and the maximum permissible magnitude of  $\xi_x(m)$  is  $\pi$  in the range  $[-\pi, \pi]$ , then equation (2.66a) becomes:

$$|\xi_x(m)|_{\max} = \pi = |-\pi \hat{u} m|_{\max} \quad (2.77)$$

or

$$|\hat{u} m|_{\max} = 1$$

For the 7-element linear array described here, the maximum value that the index m can have is 3. Therefore,

$$|\hat{u}|_{\max} = \frac{1}{3}$$

In general,

$$|\hat{u}|_{\max} = \frac{2}{M-1} \quad (2.78)$$

where  $M$  is the number of elements in the array. The corresponding angular coverage in terms of the polar coordinate angle  $\theta$  is (for  $\phi = 0$ ):

$$\theta = \sin^{-1}(|\hat{u}|_{\max}) \quad (2.79)$$

The total angular coverage is  $2\theta$ . For the case of the 7-element linear array, this corresponds to a coverage of about  $40^\circ$  out of a range of  $180^\circ$ . Figure 15 shows the expected phase angles required for beamsteering vs. element number. Figure 16 shows the wrapped angles vs. element number. It should be noted that either set of these angles (phase weights) will steer the beam to the proper direction. The difficulty with the wrapped (observed) angles is that the direction cosines  $\hat{u}$  and  $\hat{v}$  cannot be directly estimated using the methods developed in Section C.4 of this chapter. In order to unwrap the observed angles in Table 1, consider equation (2.76). It can be seen that the observed angles differ from the angles generated from equation (2.66) by an amount of  $\pm 2\pi k$  where  $k = 0, 1, 2, \dots$ . In order to unwrap the observed phase angles, it is necessary to find out which elements' phase angles have been wrapped around and by what

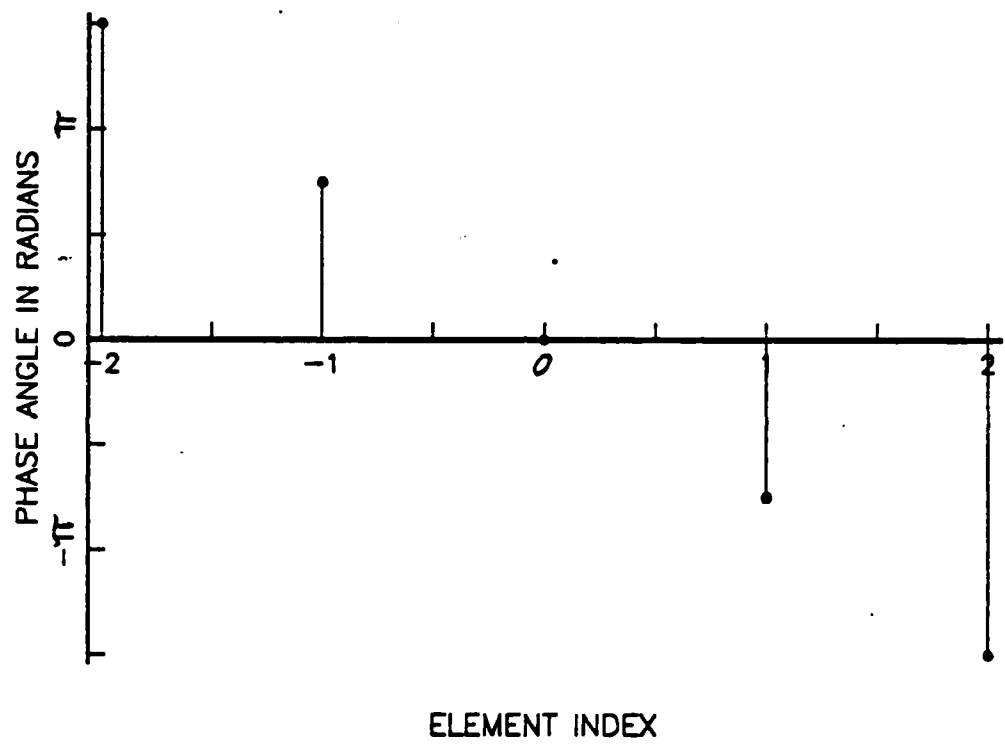


Figure 15. Phase Angles for Beamsteering

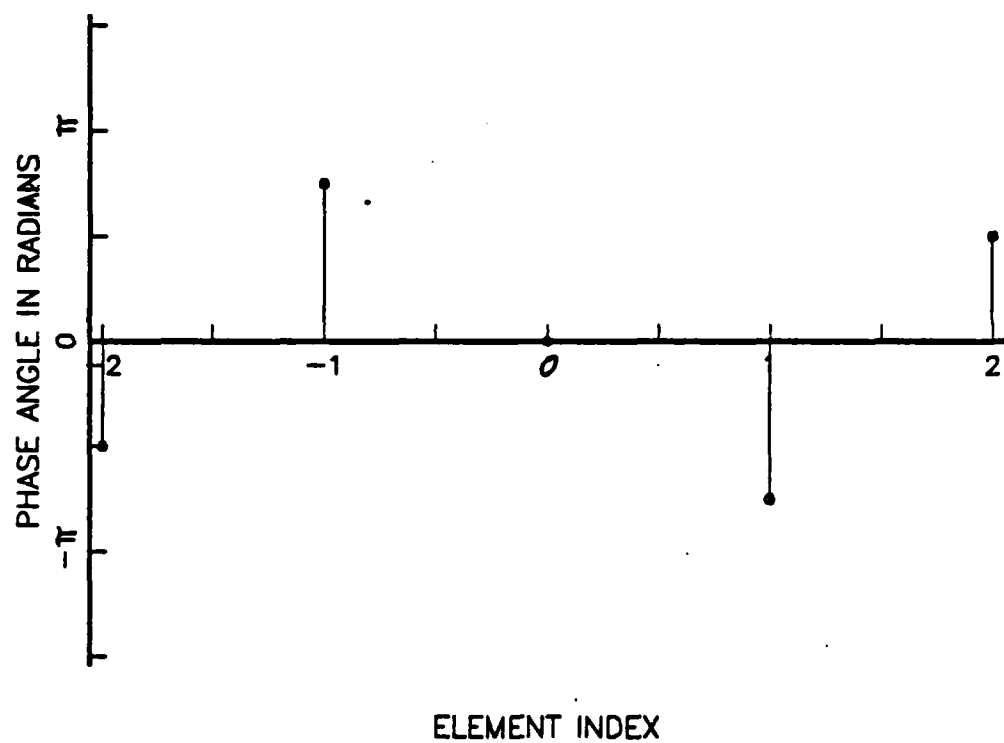


Figure 16. Wrapped-Around Phase Angles

integer multiple of  $2\pi$ . Let  $w(m)$  be the unwrap factor such that:

$$\xi_X(m) = \xi_X''(m) = \xi_X'(m) + w(m) \quad (2.80)$$

Table 2 shows (for  $\hat{u} = 0.55$  and  $d_X = \lambda/2$ ) how the implementation of equation (2.80) will yield the phase weights required for spatial resolution.

TABLE 2  
PHASE UNWRAPPING

m	-3	-2	1	0	1	2	3
$\xi_X(m)$	$1.65\pi$	$1.1\pi$	$.55\pi$	$0\pi$	$-.55\pi$	$-1.1\pi$	$-1.65\pi$
$\xi_X'(m)$	$-.35\pi$	$-.9\pi$	$.55\pi$	0	$-.55\pi$	$0.9\pi$	$0.35\pi$
$w(m)$	$+2\pi$	$+2\pi$	0	0	0	$-2\pi$	$-2\pi$
$\xi_X''(m)$	$1.65\pi$	$1.1\pi$	$.55\pi$	0	$-.55\pi$	$-1.1\pi$	$-1.65\pi$

Observe from Table 2 and equation (2.66) that the phase angles for elements  $m = -1$  and  $m = 1$  do not wrap around as long as  $d_X \leq \frac{\lambda}{2}$ . Recall also that the center element is chosen as the reference element. It is possible then after a set of steady phase weights has been computed that an estimate of the direction cosine can be computed using the phase angles at elements  $m = -1$  and  $m = 1$  in equation (2.67) below.

$$\hat{u}(m) = \frac{-\lambda \xi_x(m)}{2\pi m d_x} \quad (2.67)$$

For

$$d_x = \lambda/2,$$

$$\hat{u}(m) = \frac{-\xi_x(m)}{\pi m} \quad (2.81)$$

The estimate of direction cosine  $\hat{u}$  using only the information (phase angles) at  $m = \pm 1$  is denoted as  $\hat{u}_g$  where

$$\hat{u}_g = \frac{1}{2}[\hat{u}(1) + \hat{u}(-1)] \quad (2.82)$$

Equation (2.82) will yield a good estimate of  $\hat{u}$  as long as  $d_x \leq \frac{\lambda}{2}$ . The next step in this process of phase unwrapping is to use the result from equation (2.82) to generate a set of projected phase weights  $\{\hat{\xi}_x(m)\}$  using the following relation:

$$\hat{\xi}_x(m) = \frac{-2\pi m d_x \hat{u}_g}{\lambda} \quad (2.83)$$

Recall from equation (2.76) that a phase angle outside the range  $[-\pi, \pi]$  is mapped to an angle within  $[-\pi, \pi]$ . By examining the magnitude of the projected angle, it is possible to determine how many multiples of  $2\pi$  were lost due to the modulo  $2\pi$  property of complex numbers. The sign of  $\hat{u}_g$  and

the location of the element  $m$  determine the sign of the unwrap factor  $w(m)$ . For linear arrays with an odd number of elements, the unwrap procedure can be described as follows:

$$\text{if } (k-2)\pi \leq |\hat{\xi}(m)| < k\pi \quad (2.84)$$

and if  $|\hat{\xi}(m)|$  does not lie between the limits in equation (2.84), the value of  $k$  is decremented by two and the inequality, equation (2.84), is tested again until  $|\hat{\xi}(m)|$  falls within a  $2\pi$  interval, then

$$|w(m)| = (k-1)\pi \quad (2.85)$$

For an  $M$ -element (odd) array, the initial value of  $k$  is  $(\frac{M-1}{2})$ . The sign of  $w(m)$  is determined by:

$$\text{sign } w(m) = -\text{sign } (m) \text{ sign } (\hat{u}_g) \quad (2.86)$$

where:

$$m = -(\frac{M-1}{2}), \dots, -2, -1, 0, 1, \dots, (\frac{M-1}{2}),$$

i.e., using the center element as the reference. A similar procedure can be utilized in an array with an even number of elements. The reference used should then be the point between the two center elements since there is no need for the

reference point to coincide with the location of a sensor element. This choice of reference takes full advantage of the resulting symmetry. From Table 2, it can be seen that only half of the elements need to be examined using equations (2.84)-(2.86). The unwrap factors  $\{w(m)\}$  for the other half are simply the negative of the first half. This unwrap procedure is good for the two array configurations discussed in Sections 3a. and 3c. of this chapter. The unwrap procedure for the two-dimensional array is similar but the computation is a little more involved. The unwrapping procedure for the linear array in the y-direction is identical with the substitution  $d_x \rightarrow d_y$ ,  $m \rightarrow n$ ,  $\xi_x(m) \rightarrow \xi_y(n)$ , ..., etc.

#### b. Two-dimensional Array Unwrapping

The proper phase weights to steer a beam to  $(\hat{u}, \hat{v})$  are given by:

$$\xi_{xy}(m,n) = \frac{-2\pi}{\lambda}(\hat{u} m d_x + \hat{v} n d_y) \quad (2.87)$$

The unwrapping procedure is best illustrated by considering the following example. Consider the case  $(\hat{u}, \hat{v}) = (-0.7, +0.7)$  and  $d_x = d_y = \lambda/2$ . Equation (2.87) then becomes:

$$\begin{aligned} \xi_{xy}(m,n) &= -\pi(\hat{u}m + \hat{v}n) \\ &= -\pi(-0.7m + 0.7n) \end{aligned} \quad (2.88)$$

Assume also that we are given a planar array with M elements in the x-direction and N elements in the y-direction (the corresponding element indices are  $(x,y) \rightarrow (m,n)$ , with both M and N equal to 5. For the sake of symmetry, let the element indices run as follows:

$$m = -(\frac{M-1}{2}), -(\frac{M-1}{2})+1, \dots, 0, 1, \dots, (\frac{M-1}{2})$$

$$n = -(\frac{N-1}{2}), -(\frac{N-1}{2})+1, \dots, 0, 1, \dots, (\frac{N-1}{2})$$

In this case, for  $M = 5$ ,

$$m = -2, -1, 0, 1, 2.$$

Similarly, for the orthogonal direction,

$$n = -2, -1, 0, 1, 2.$$

The obvious choice of reference element is  $(m,n) = (0,0)$ , i.e., the center element. The desired phase weights for this example are given in Table 3.

The phase weights marked within the two triangles in Table 3 will be wrapped around, so the actual observed phases when the phase weights reach steady state are tabulated in Table 4.

TABLE 3

DESIRED PHASE WEIGHTS  $\{\xi_{xy}(m,n)\}$  GIVEN  
THAT  $u = -0.7, v = +0.7$

n						
2	$-2.8\pi$	$-2.1\pi$	$-1.4\pi$	$-0.7\pi$	0	
1	$-2.1\pi$	$-1.4\pi$	$-0.7\pi$	0	$0.7\pi$	
0	$-1.4\pi$	$-0.7\pi$	0	$0.7\pi$	$1.4\pi$	
-1	$-0.7\pi$	0	$0.7\pi$	$1.4\pi$	$2.1\pi$	
-2	0	$0.7\pi$	$1.4\pi$	$2.1\pi$	$2.8\pi$	
	-2	-1	0	1	2	m

TABLE 4

OBSERVED PHASES OF THE STEADY STATE  
ADAPTIVE WEIGHTS  $\xi'_{xy}(m,n)$

n						
2	$-0.8\pi$	$-0.1\pi$	$0.6\pi$	$-0.7\pi$	0	
1	$-0.1\pi$	$0.6\pi$	$-0.7\pi$	0	$0.7\pi$	
0	$0.6\pi$	$-0.7\pi$	0	$0.7\pi$	$-0.6\pi$	
-1	$-0.7\pi$	0	$0.7\pi$	$-0.6\pi$	$0.1\pi$	
-2	0	$0.7\pi$	$-0.6\pi$	$0.1\pi$	$0.8\pi$	
	-2	-1	0	1	2	m

Let  $w(m,n)$  be the two-dimensional unwrap factor, i.e., the unwrapped phase is:

$$\xi_{xy}(m,n) = \xi''_{xy}(m,n) = \xi'_{xy}(m,n) + w(m,n) \quad (2.89)$$

By comparing  $\{\xi_{xy}(m,n)\}$  in Table 3 with  $\{\xi'_{xy}(m,n)\}$  in Table 4, it can be seen that  $w(m,n)$  must be equal to the tabulated values in Table 5.

TABLE 5  
UNWRAP FACTORS  $w(m,n)$

n					
2	$-2\pi$	$-2\pi$	$-2\pi$	0	0
1	$-2\pi$	$-2\pi$	0	0	0
0	$-2\pi$	0	0	0	$2\pi$
-1	0	0	0	$2\pi$	$2\pi$
-2	0	0	$2\pi$	$2\pi$	$2\pi$
	-2	-1	0	1	2
					m

To generate  $w(m,n)$ , estimates of the direction cosines  $\hat{u}$  and  $\hat{v}$  must be computed using elements at  $m = \pm 1$  and  $n = \pm 1$ . Let  $\hat{u}_g$  and  $\hat{v}_g$  be those estimates obtained using the point by point method below:

$$\hat{u}_g = \frac{1}{2}[\hat{u}(1) + \hat{u}(-1)] \quad (2.90)$$

$$\hat{v}_g = \frac{1}{2}[\hat{v}(1) + \hat{v}(-1)] \quad (2.91)$$

For  $d_x = d_y = \lambda/2$ , equation (2.88) can be applied to compute the projected phases  $\{\hat{\xi}_{xy}(m,n)\}$  by the relation:

$$\hat{\xi}_{xy}(m,n) = -\pi\{\hat{u}_g m + \hat{v}_g n\} \quad \text{for all } m \text{ and } n \quad (2.92)$$

The set of projected phases (angles) are then examined to decide the proper unwrap factor for a particule element  $(m,n)$ . The logic is as follows: for each  $n$ , all elements  $m$  are examined.

$$\text{Check} \quad (k-2)\pi \leq |\hat{\xi}_{xy}(m,n)| < k\pi \quad (2.93)$$

and if  $|\hat{\xi}_{xy}(m,n)|$  does not lie between the limits, then  $k$  is decremented by two and equation (2.93) is tested again. If  $|\hat{\xi}_{xy}(m,n)|$  does lie between the limits, then

$$|w_{xy}(m,n)| = (k-1)\pi \quad (2.94)$$

This procedure applies when  $M$  is odd and the initial value of  $k$  is  $(\frac{M-1}{2})$ . The sign of  $w(m,n)$  is determined by:

$$\text{sign}[w(m,n)] = -\text{sign}[\text{sign}(m)\text{sign}(\hat{u}_g) + \text{sign}(n)\text{sign}(\hat{v}_g)] \quad (2.95)$$

where:

$$m = -(\frac{M-1}{2}), \dots, -1, 0, 1, \dots, (\frac{M-1}{2})$$

$$n = -(\frac{N-1}{2}), \dots, -1, 0, 1, \dots, (\frac{N-1}{2})$$

For the next value of  $n$ , equations (2.93), (2.94), and (2.95) are repeated for all values of  $m$ . This continues until the last value of  $n$  is reached. It is possible though to examine only half of the planar array since the unwrap factors for the other half are the negative of that of the first half. To ensure symmetry about the reference element, it is necessary to rotate the phase angle at the reference element to zero. This can be accomplished by multiplying the phase weights of all  $M \times N$  elements by the complex conjugate of the reference phase weight, i.e.,

$$cd_i(m,n) \leftarrow cd_i(m,n) cd_i^*(m_0, n_0) \quad (2.96)$$

where  $m$  and  $n$  are the indices locating the reference element. This operation will ensure that the unwrapping procedure will work properly. For linear array phase weights, this phase centering should also be completed before unwrapping. The equations are:

$$c_i(m) \leftarrow c_i(m) c_i^*(m_0) \quad (2.97)$$

$$d_i(n) \leftarrow d_i(n) d_i^*(n_0) \quad (2.98)$$

where  $m_0$  is the index locating the reference element of the linear array along the x-direction and  $n_0$  is the index locating the reference element of the linear array along the y-direction.

## 6. Summary

The original complex LMS adaptive filter [Ref. 1] requires three necessary modifications to make it useful for estimating the direction cosines of an incident plane wave. Without the following modifications, accurate spatial resolution is not possible:

- normalization of the adaptive complex weights (phasors) to unity magnitude after each iteration.
- unwrapping of the observed steady state phase angles to extend the spatial coverage to the full range of  $u$  and  $v$ .
- allowing the feedback coefficient  $\mu$  to decrease with increasing iteration number to achieve convergence to an optimal set of phase weights and to realize a robust filter.

## D. NOISE MODEL

In the SONAR environment, the ambient noise field is a composite of many different noise sources. Therefore, using the Central Limit Theorem [Ref. 13], the ambient noise can be modeled quite adequately as additive white Gaussian noise. Intentional jamming is not considered in this thesis. However, the use of an adaptive filter to place a null at the

spatial location of a jamming signal has been studied extensively [Refs. 2,4,15]. The noise corrupted received signal is given by:

$$r(\ell,m,n) = y(\ell,m,n) + n(\ell,m,n) \quad (2.99)$$

where  $y(\ell,m,n)$  is the sampled signal represented by equation (2.26) and  $n(\ell,m,n)$  is white Gaussian noise time samples with zero mean and noise power  $\sigma_N^2$ . If  $A$  is the signal amplitude (see equation (2.26)), then the signal-to-noise ratio is given by:

$$\text{SNR} = \frac{A^2}{\sigma_N^2} \quad (2.100)$$

or

$$(\text{SNR})_{\text{dB}} = 10 \log_{10} (\text{SNR}) \text{ dB} \quad (2.101)$$

The performance of the frequency domain LMS adaptive filter was tested for various signal-to-noise ratios. The noise environment is assumed to be stationary during the look interval of the SONAR system.

### III. LOW FREQUENCY PASSIVE SONAR TARGET LOCALIZATION

The objectives in passive SONAR are to detect and possibly classify noise sources in the ocean. Most of the noise generated by vessels is concentrated in the low frequency range (30-1K Hz). Acoustic energy in this frequency range is capable of long range propagation and, as a result, most long range detection systems in the underwater environment operate at these low frequencies. Propeller cavitation, machinery noise, and wake are the major sources of such noise. Under certain situations, very long range detection has been demonstrated in this frequency range. In a long range detection scenario, knowledge of the elevation/depression angle is necessary to resolve potential range ambiguities in convergence zone (CZ) problems. Therefore, the use of a planar array is well justified.

A computer program was implemented using the VS APL language to test the performance of the LMS adaptive filter in a noisy passive environment. The array size used in the simulation is small compared to most modern systems but the other parameters are set to simulate a very realistic passive SONAR. The APL language is used because of its large library of advanced signal processing functions and its interactive mode of operation which allows for rapid program development. The major disadvantage of the APL language is

its slower speed of execution compared to running a compiled Fortran program that performs the same functions. This is not a serious problem, however, for the research of this thesis.

#### A. PROBLEM STATEMENT

A low frequency acoustic signal from a far-field source is received by a planar array in a noisy underwater environment. The noise is assumed to be Gaussian and uncorrelated with the signal. It is also assumed that the noise between elements is uncorrelated. The planar array has a square structure with  $M = 5$  elements in the x-direction and  $N = 5$  elements in the y-direction. The element spacing is set to one-half the wavelength of the maximum frequency of the system's operating range. The geometry of the problem is shown in Figure 17 [Ref. 18]. The system parameters are:

- Signal:  $A \cos(2\pi ft)$ , where  $A$  is the amplitude and  $f$  is the frequency
- Integration time: 0.5 seconds ( $T_O$ )
- Frequency resolution: 2 Hz ( $1/T_O = f_O$ )
- Number of samples:  $128 = 2^7$  ( $L$ )
- Number of sensor elements in the x-direction: 5 ( $M$ )
- Number of sensor elements in the y-direction: 5 ( $N$ )
- Speed of sound: 1500 meters/second ( $c_O$ )
- Sampling rate: 256 samples/second ( $f_s$ )
- Frequency range: 0-128 Hz
- Number of frequency bins: 128

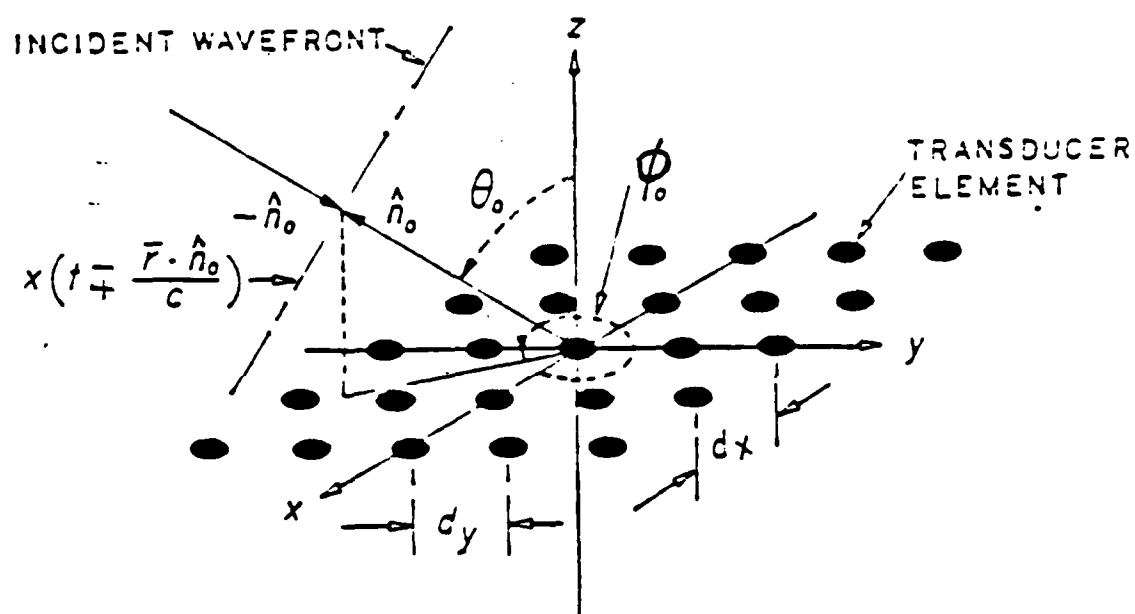


Figure 17. System Geometry [Ref. 18:p. 19]

- Elements spacing: 7.5 meters ( $d_x$  and  $d_y$  equal)
- Noise model: additive white Gaussian  $\sim N(0, \sigma_N^2)$
- Number of noise samples per sample function: 3200,  
i.e.,  $L \times M \times N = 128 \times 5 \times 5$

The signal used in the simulation is a 100 Hz sinusoid corrupted by white Gaussian noise. A total of 128 samples are taken for each processing period of 0.5 seconds. This corresponds to 256 samples per second which satisfies the Nyquist sampling theorem [Refs. 12,16,17]. The maximum observed frequency in this case is 128 Hz. The 100 Hz signal will center in bin number 50 for this simulation. Frequency bin numbers 64-127 correspond to the negative frequencies [Ref. 16]. The element spacing of 7.5 meters is the maximum allowable separation for the 100 Hz signal to avoid grating lobes in the far-field directivity beam pattern. The speed of sound is the speed in the proximity of the planar array.

## B. SIMULATION

Given the system parameters stated in Section A, and a 128 point DFT, a 100 Hz sinusoidal signal will be centered in frequency bin number 50. The logical flow graph of the simulation program is shown in Figure 18. The principle of superposition allows different frequency bins to be processed independently. However, if the same frequency is emitted from two or more spatial locations, the LMS adaptive filter will lock on to the one closest to boresight. Complete

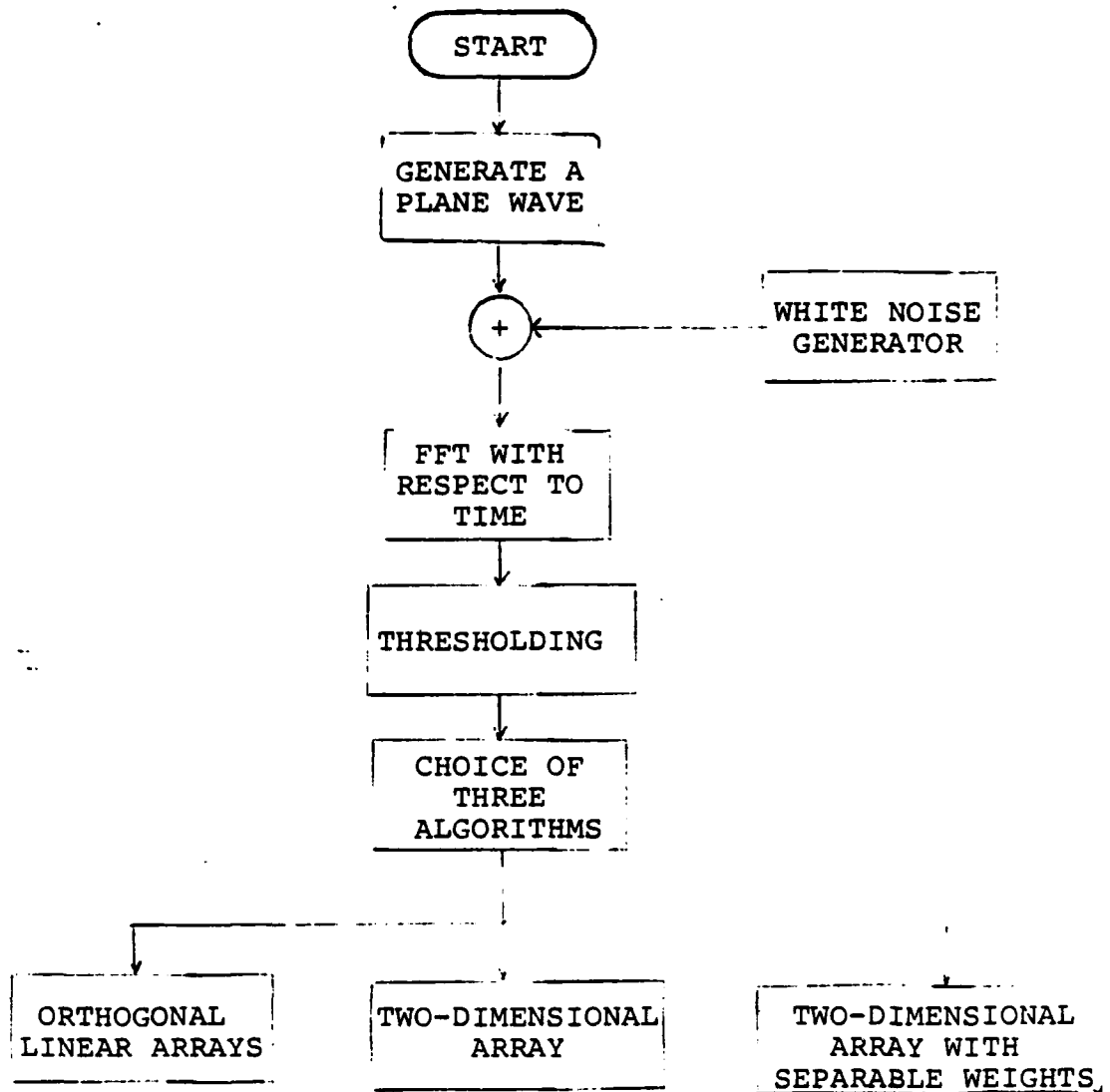


Figure 18. Logical Flow Graph of the Simulation Program for the Low Frequency Passive Detection Problem

documentation of the simulation program for this case can be found in Appendix B. The outputs of the simulation program are the estimated direction cosines  $u$  and  $v$ . The RMS error is defined as:

$$\epsilon = (\Delta u^2 + \Delta v^2)^{1/2} \quad (3.1)$$

where:

$$\Delta u = \hat{u} - u \quad (3.2)$$

$$\Delta v = \hat{v} - v \quad (3.3)$$

where  $u$  and  $v$  are the actual direction cosines. This measure of error is consistent with the least-squares criterion used in estimating  $u$  and  $v$ . If the estimate of the spherical coordinates  $(\hat{\theta}, \hat{\phi})$  are required, the following transformations will transform  $(\hat{u}, \hat{v})$  to  $(\hat{\theta}, \hat{\phi})$  [Ref. 5]:

$$\hat{\theta}(\hat{u}, \hat{v}) = \sin^{-1}[(\hat{u})^2 + (\hat{v})^2]^{1/2} \quad (3.4)$$

and

$$\hat{\phi}(\hat{u}, \hat{v}) = \tan^{-1}(\hat{v}/\hat{u}) \quad (3.5)$$

It should be noted that the transformation from  $(\hat{u}, \hat{v})$  to  $(\hat{\theta}, \hat{\phi})$  is nonlinear. A particular value of the RMS error

in equation (3.1) can be due to infinitely many different values of  $\hat{\theta}$  and  $\hat{\phi}$ , that is, given an RMS error  $\epsilon$ , there is no unique set of spherical angle estimates. The spherical angle estimates  $(\hat{\theta}, \hat{\phi})$  depend on the values of both  $\hat{u}$  and  $\hat{v}$ . Evaluating the total differential of equation (3.4) and equation (3.5) yields:

$$d\hat{\theta} = \frac{\hat{u}d\hat{u} + \hat{v}d\hat{v}}{\sqrt{(\hat{u}^2 + \hat{v}^2)(1 - (\hat{u}^2 + \hat{v}^2))}} \quad (3.6)$$

and

$$d\hat{\phi} = \frac{\hat{u}}{\hat{u}^2 + \hat{v}^2} (d\hat{v} - \frac{\hat{v}d\hat{u}}{\hat{u}}) \quad (3.7)$$

Replacing  $d\hat{\theta}$  by  $\Delta\theta$ ,  $d\hat{\phi}$  by  $\Delta\phi$ ,  $d\hat{u}$  by  $\Delta u$  and  $d\hat{v}$  by  $\Delta v$  results in the following:

$$\Delta\theta \cong \frac{\hat{u}\Delta u + \hat{v}\Delta v}{\sqrt{(\hat{u}^2 + \hat{v}^2)(1 - (\hat{u}^2 + \hat{v}^2))}} \quad (3.8)$$

$$\Delta\phi \cong \frac{\hat{u}}{\hat{u}^2 + \hat{v}^2} (\Delta v - \frac{\hat{v}\Delta u}{\hat{u}}) \quad (3.9)$$

### C. RESULTS

Three versions of the frequency domain LMS adaptive filter were discussed in Chapter II. The performance of each will be presented here.

## 1. Orthogonal Linear Arrays

This configuration uses only  $M+N-1$  elements. The parameters used for the simulation are as follows:

Signal -  $\cos 2\pi(100)t$  (bin number 50)

Number of iterations (I) - 75

Initial feedback coefficient ( $\mu_x$ ) - 0.0005

Initial feedback coefficient ( $\mu_y$ ) - 0.0005

Scale factor for  $\mu_x$  and  $\mu_y$  ( $\alpha_s$ ) - 0.909 (see Appendix A)

Input SNR at single array element, i.e., SNR at FFT input - 0 dB

Incident angles ( $\theta, \phi$ ) - ( $55^\circ, 35^\circ$ ) (see Figure 17)

The corresponding direction cosines ( $u, v$ ) - (0.67101, 0.46985)

Figures 19 and 20 show the convergence characteristics of the complex LMS adaptive filter vs. iteration number  $i$ . The solid horizontal lines are the true values of direction cosines  $u$  and  $v$ . The oscillations in the beginning of the adaptation are due to the large initial values of  $\mu_x$  and  $\mu_y$ . The feedback coefficients  $\mu_x$  and  $\mu_y$  are scaled down recursively by the scale factor via the rule described in Appendix A which is rewritten below:

$$\mu_x(i) = \mu_x(i-1)\alpha_s \quad (3.10a)$$

and

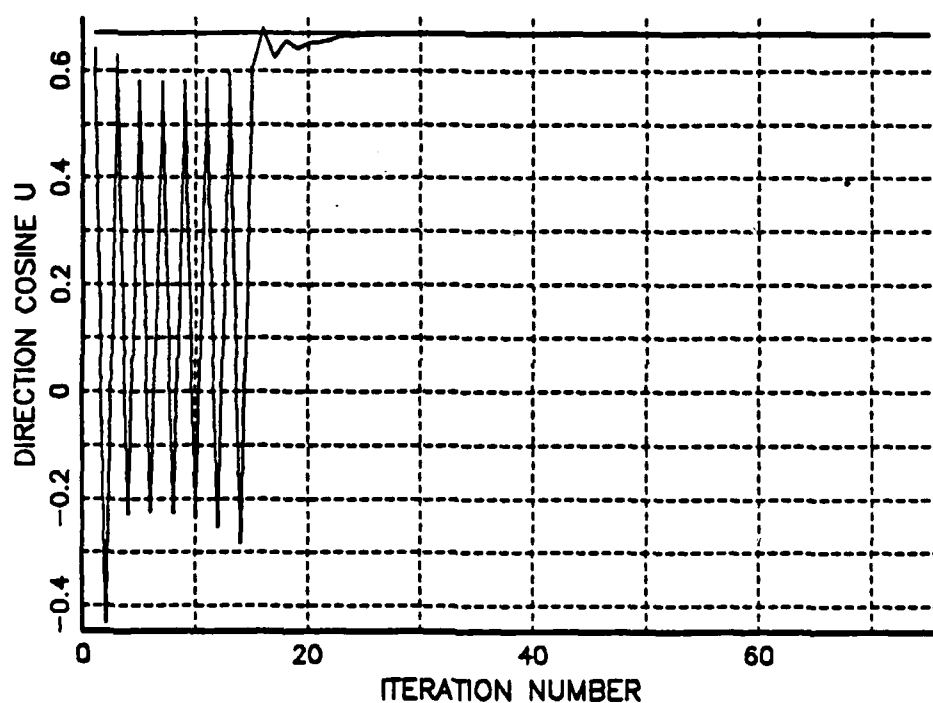


Figure 19. Convergence Characteristics of the LMS Adaptive Filter using the Orthogonal Linear Arrays Configuration in Estimating the Direction Cosine  $u$  at an Input SNR of 0 dB

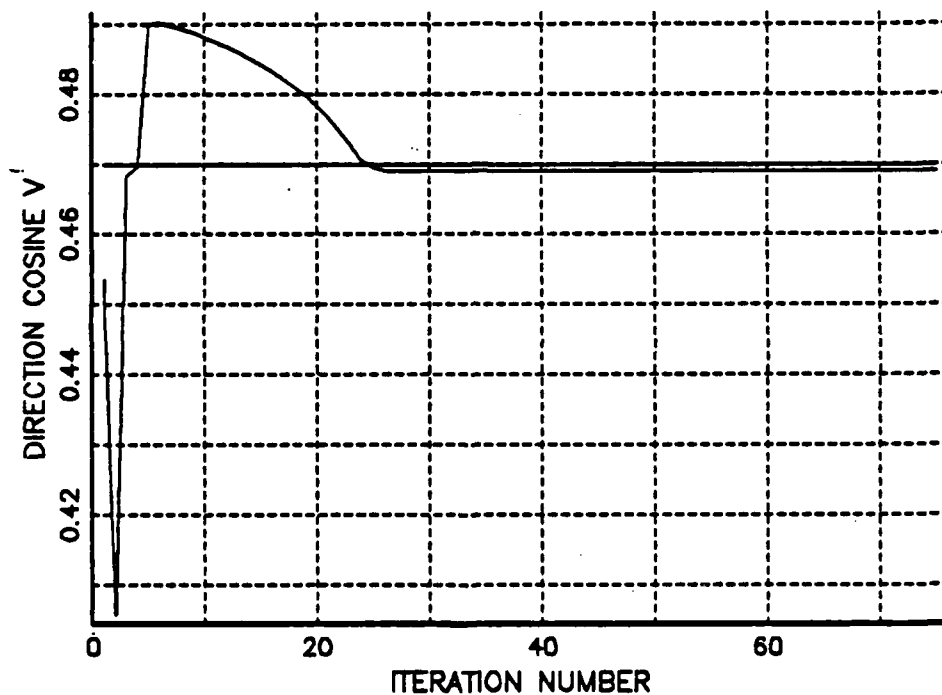


Figure 20. Convergence Characteristics of the LMS Adaptive Filter using the Orthogonal Linear Arrays Configuration in Estimating the Direction Cosine  $v$  at an Input SNR of 0 dB

$$\mu_y(i) = \mu_y(i-1)\alpha_s \quad (3.10b)$$

Convergence to the steady state occurred in fewer than 35 iterations in both cases. Figure 21 shows the error in estimating  $u$  and  $v$  using equation (3.1) vs. iteration number. The use of a constant feedback coefficient requires a much longer iteration period and results in less accuracy (see Appendix A). The chosen initial values of  $\mu_x$  and  $\mu_y$  are outside the bound of the convergence coefficient described in Appendix A. However, the convergence coefficients are decreased rapidly using equation (3.10). This choice of  $\mu_x$  and  $\mu_y$  shows that the LMS adaptive filter with decreasing convergence coefficient(s) is very robust. Table 6 summarizes the simulation results for a particular sample function of noise.

## 2. Two-dimensional Array

This version uses all  $M \times N$  elements and the complex weights are not assumed to be separable. The parameters used in the simulation are:

Signal -  $\cos 2\pi(100)t$  (bin number 50)

Number of iterations (I) - 75

Initial convergence coefficient - 0.001

scale factor ( $\alpha_s$ ) - 0.909

Input SNR at single array element, i.e., SNR at FFT input - 0 dB

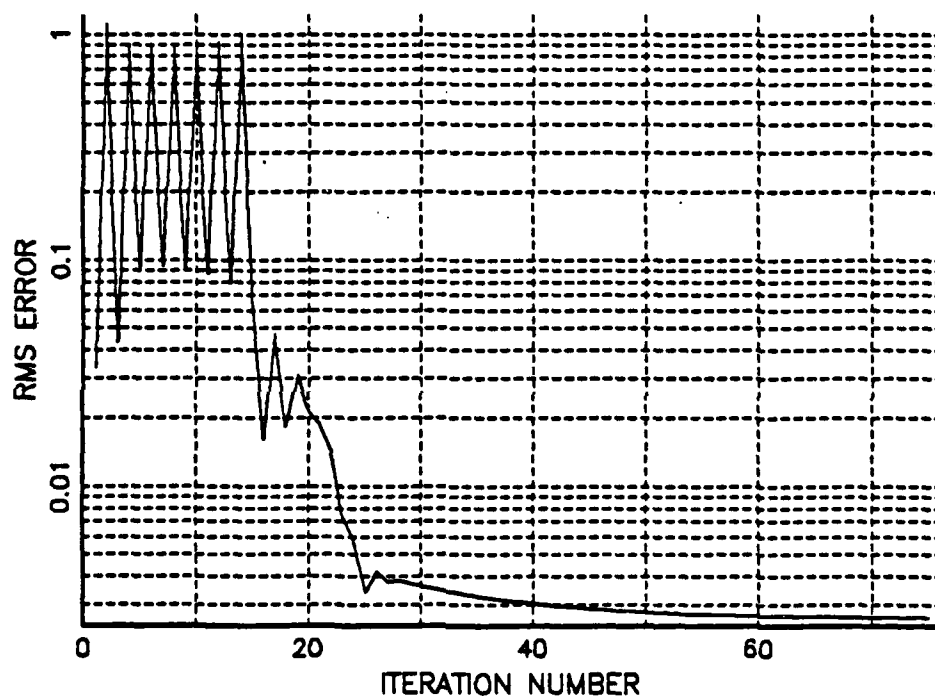


Figure 21. The RMS Error in Estimating  $u$  and  $v$  Using the Orthogonal Linear Arrays Configuration at an Input SNR of 0 dB

TABLE 6

SUMMARY OF COMPLEX LMS ADAPTIVE FILTER  
PERFORMANCE FOR THE ORTHOGONAL LINEAR  
ARRAY CONFIGURATION AT SNR = 0 dB

	Simulation Values
$u$	0.671010
$v$	0.469846
$\hat{u}$	0.695675
$\hat{v}$	0.466038
$\Delta u = \hat{u} - u$	$2.4665 \times 10^{-2}$
$\Delta v = \hat{v} - v$	$-3.808 \times 10^{-3}$
$\epsilon = (\Delta u^2 + \Delta v^2)$	0.024957
$\theta$	$55^\circ$
$\hat{\theta}$	$54.783^\circ$
$\phi$	$35^\circ$
$\hat{\phi}$	$33.818^\circ$

Incident angle  $(\theta, \phi)$  -  $(55^\circ, 35^\circ)$

Corresponding  $(u, v)$  -  $(0.67101, 0.46985)$

Figures 22 and 23 show the convergence characteristics of the two-dimensional array configuration of the complex LMS adaptive filter vs. iteration number  $i$ .

Figure 24 plots the RMS error in estimating  $u$  and  $v$  (see equation (3.1)). The results of the simulation for a particular sample function of noise are summarized in Table 7.

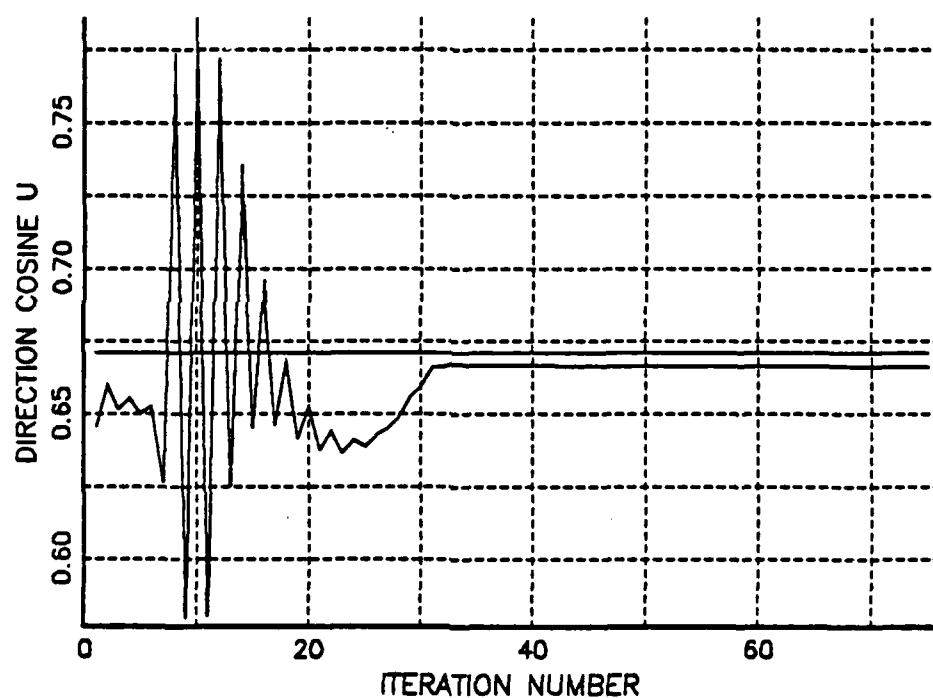


Figure 22. Convergence Characteristics of the LMS Adaptive Filter for the Two-dimensional Array in Estimating the Direction Cosine  $u$  at an Input SNR of 0 dB

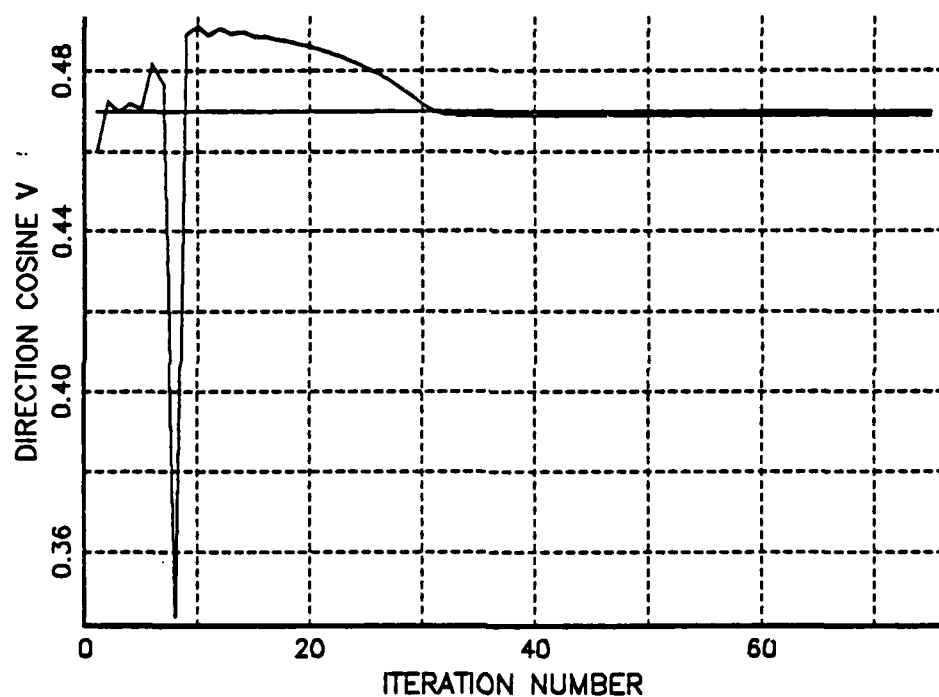


Figure 23. Convergence Characteristics of the LMS Adaptive Filter for the Two-Dimensional Array in Estimating the Direction Cosine  $v$  at an Input SNR of 0 dB

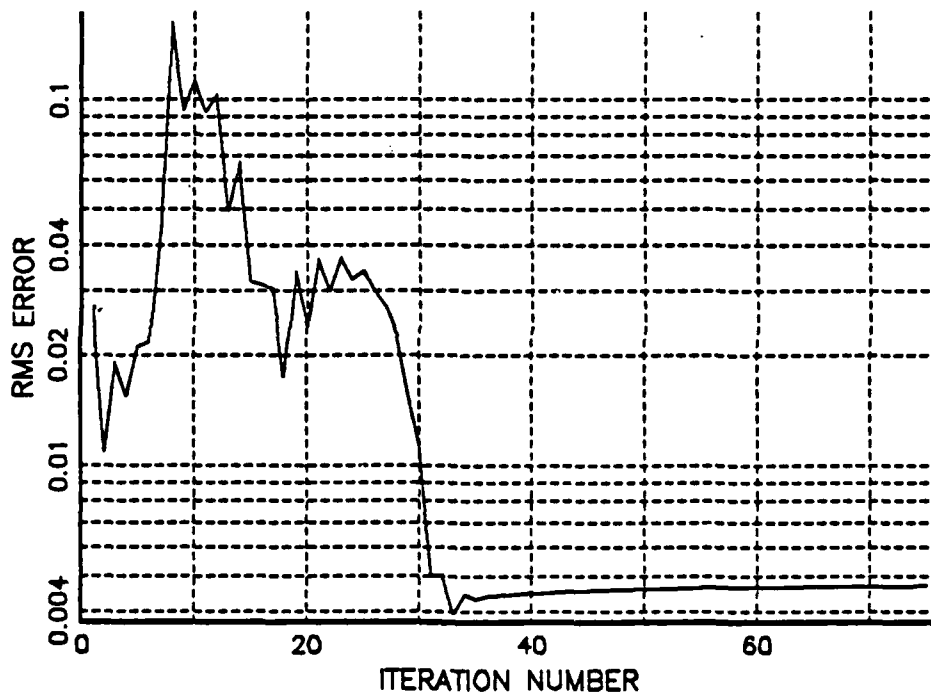


Figure 24. The RMS Error in Estimating  $u$  and  $v$  Using the Two-dimensional Array at an Input SNR of 0 dB

TABLE 7

SUMMARY OF COMPLEX LMS ADAPTIVE FILTER PERFORMANCE  
FOR THE TWO-DIMENSIONAL ARRAY AT SNR = 0 dB

	Simulation Values
u	0.67101
v	0.46985
$\hat{u}$	0.68442
$\hat{v}$	0.46569
$\Delta u$	$1.341 \times 10^{-2}$
$\Delta v$	$-4.16 \times 10^{-3}$
$\epsilon$	$1.404 \times 10^{-2}$
$\theta$	55°
$\hat{\theta}$	55.876°
$\phi$	35°
$\hat{\phi}$	34.232°

### 3. Two-dimensional Array with Separable Weights

This configuration assumes that the complex weights are separable, i.e.,  $cd(m,n) = c(m)d(n)$ . The simulation parameters are the same as those used in the two-dimensional array case discussed in the previous section. Figures 25 and 26 show the convergence characteristics of this configuration. Figure 27 shows the RMS error versus number of iterations. The summary for this run is in Table 8. An alternate way to illustrate the performance of the complex LMS adaptive filter is a plot of RMS error vs. input SNR at

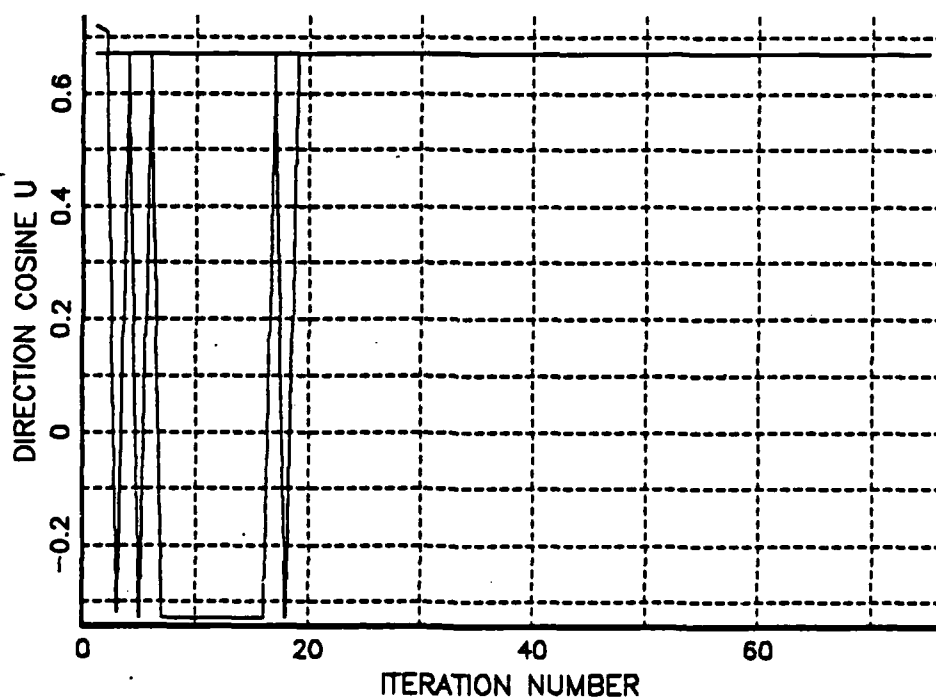


Figure 25. Convergence Characteristics of the LMS Adaptive Filter for the Two-dimensional Array with Separable Weights in Estimating the Direction Cosine  $u$  at an Input SNR of 0 dB

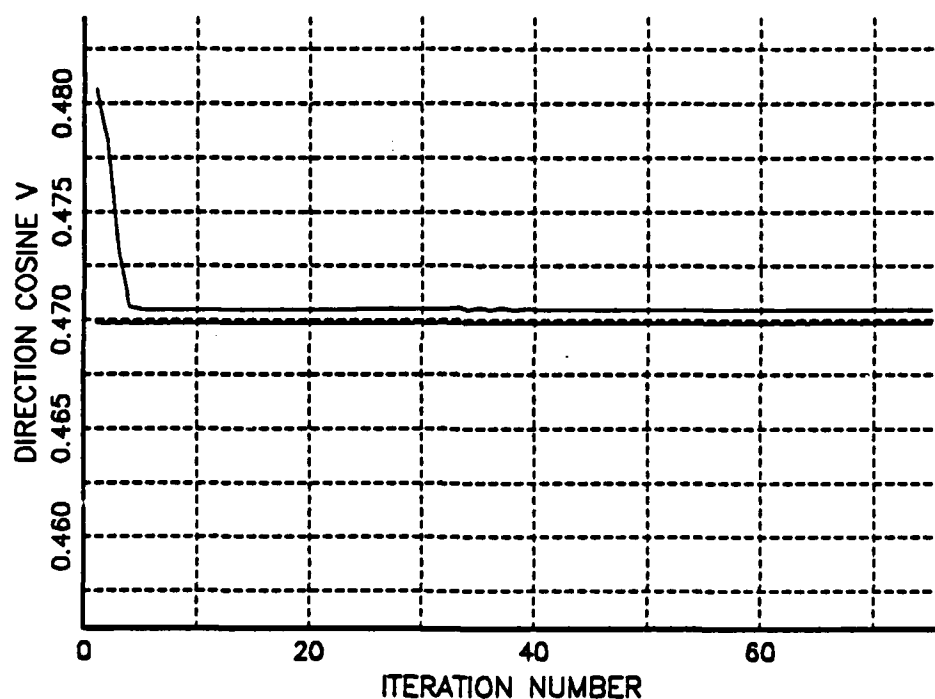


Figure 26. Convergence Characteristics of the LMS Adaptive Filter for the Two-dimensional Array with Separable Weights in Estimating the Direction Cosine  $v$  at an Input SNR of 0 dB

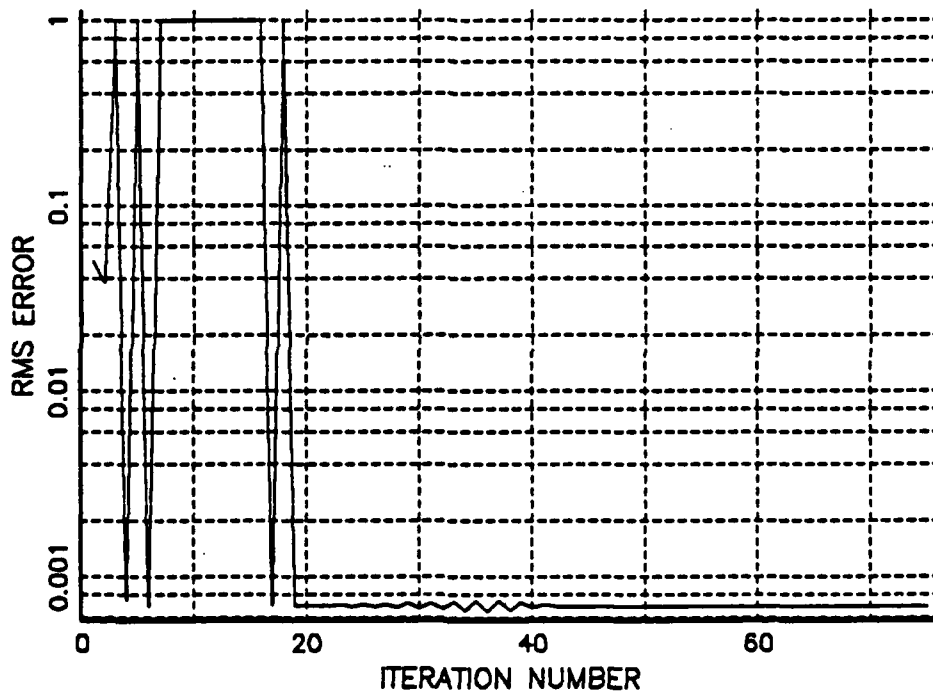


Figure 27. The RMS Error in Estimating the Direction Cosines  $u$  and  $v$  Using the Two-dimensional Array with Separable Weights at an Input SNR of 0 dB

TABLE 8

SUMMARY OF COMPLEX LMS ADAPTIVE FILTER PERFORMANCE  
FOR THE TWO-DIMENSIONAL ARRAY WITH SEPARABLE  
WEIGHTS AT SNR = 0 dB

	Simulation Values
u	0.67101
v	0.46985
$\hat{u}$	0.66304
$\hat{v}$	0.47353
$\Delta u$	$-7.97 \times 10^{-3}$
$\Delta v$	$3.68 \times 10^{-3}$
$\epsilon$	$8.78 \times 10^{-3}$
$\theta$	55°
$\hat{\theta}$	54.565°
$\phi$	35°
$\hat{\phi}$	35.534°

a single array element (SNR at FFT input). Figure 28 shows these curves for all three configurations.

#### D. SUMMARY

The algorithm that assumes separable complex weights shows better performance over the prescribed SNR range. The improvement of performance of all three algorithms with increasing SNR is evident from Figure 28. Since each noise sample function has a total of 3200 independent samples, the RMS error versus SNR curve is rather smooth. If several sample

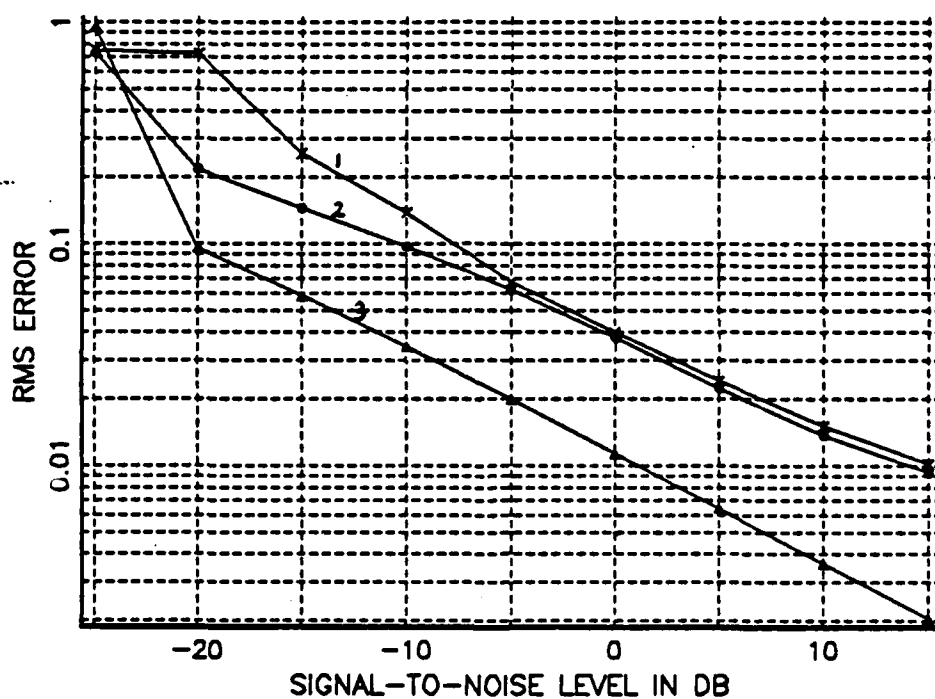


Figure 28. The RMS Error in Estimating  $u$  and  $v$  Versus Input SNR.  
 Curve 1: Orthogonal Linear Arrays Configuration  
 Curve 2: Two-dimensional Array  
 Curve 3: Two-dimensional array with Separable Weights

functions are averaged, the slight 'humps' in Figure 28 can be smoothed out further. The RMS error quantity is analogous to that of a 'miss distance' on a rectangular grid.

#### IV. PULSE COMMUNICATION [Ref. 18]

The simulation results of two cases are presented in this chapter. They are:

- Homogeneous medium case, in which the output electrical signal data at each array element is produced by the ocean communication channel simulation computer program [Ref. 19]. Figure 29 shows the system geometry of this case [Ref. 18]. Note that the ray path from transmit to receive array is a straight path.
- Inhomogeneous medium case, in which the ray path is bent due to the variable sound-speed profile. Thus, the apparent direction of arrival viewed from the receive array is different from the previous case. Figure 30 shows the system geometry of the inhomogeneous medium case [Ref. 18].

From the analysis of Chapter II, it can be seen that the LMS adaptive filter should be able to phase align a planar array to point in the direction of arrival. The signals used for this simulation are a CW pulse and a LFM pulse. These are very common signals used in the SONAR environment. Information is carried by the modulation of these pulses. The Fortran program used to simulate this problem is documented in Appendix C. Blount [Ref. 18] studied the effect of model-based cophasing on the probability of detection of a single pulse. The amount of cophasing is determined by the system geometry and deterministic ray bending. It was shown that by applying the phase weights generated by considering those factors, the performance of a correlator receiver was improved markedly. Analysis done on those

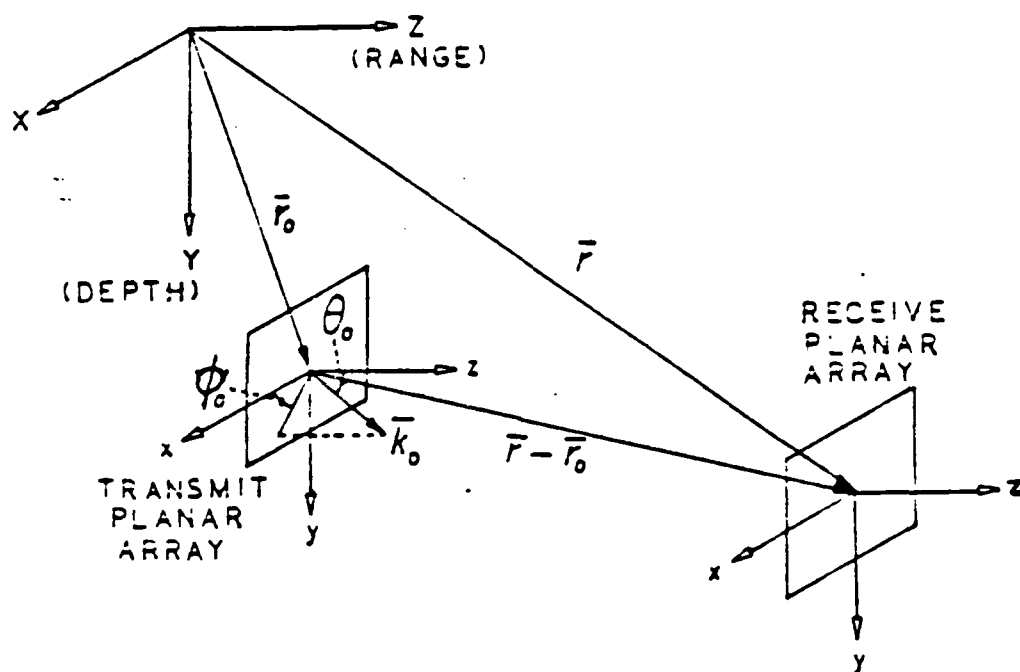


Figure 29. System Geometry for the Homogeneous Medium Case [Ref. 18:p. 16]

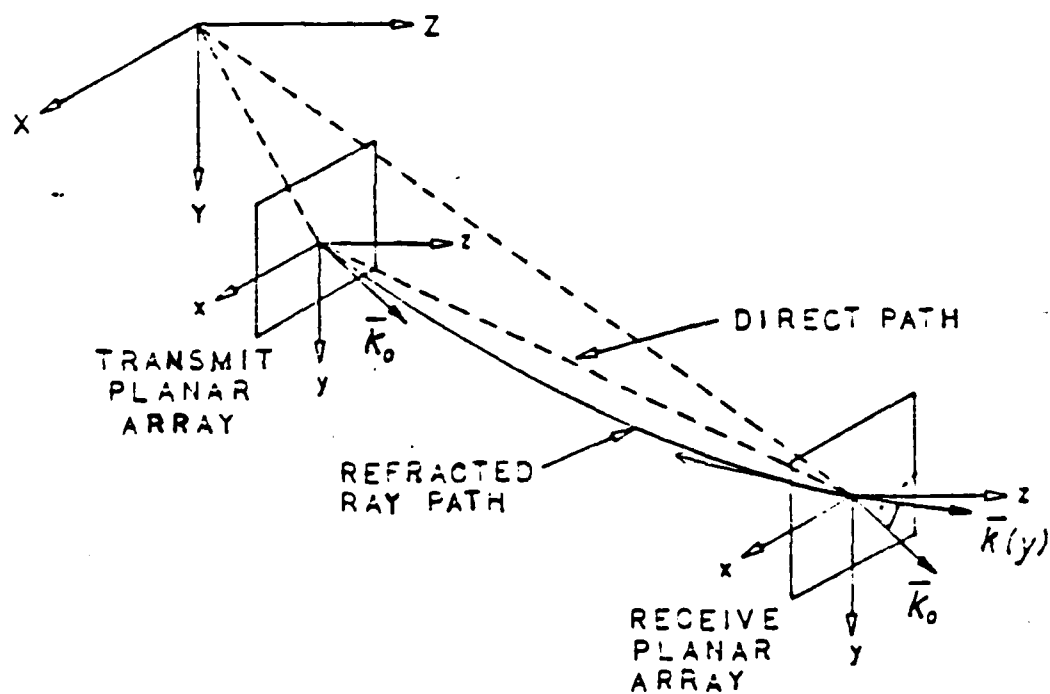


Figure 30. System Geometry for the Inhomogeneous Medium Case [Ref. 18:p. 17]

steering phase weights showed that the main beam of the array directivity pattern was indeed steered to the direction of actual arrival instead of line of sight.

#### A. TRANSMIT WAVEFORMS [Ref. 18]

Two types of waveforms were used to test the LMS adaptive algorithm.

##### 1. Rectangular-envelope CW Pulse

The signal presented to the processor is a quadrature demodulated complex envelope of the CW pulse [Refs. 5, 18].

$$\tilde{z}(t) = \sum_{k=-K}^K z_n e^{jk(2\pi f_0)t} \quad (4.1)$$

where " $\tilde{\cdot}$ " denotes complex envelope.

The pulse repetition frequency is the same as the fundamental frequency  $f_0$  of the finite ( $K$  harmonics) frequency spectrum from which the pulse is synthesized. The pulse duty cycle is arbitrarily set to 0.5. The complex Fourier series coefficients  $z_n$  used to synthesize the complex envelope of the CW pulse are obtained from a closed-form expression for the complex-valued continuous spectrum. The Fourier coefficients are obtained by evaluating the closed-form expression for the continuous spectrum at discrete frequencies corresponding to integer multiples of the

fundamental frequency. The following specific transmit signal parameters were used in all CW pulse simulations:

- Amplitude (A): 40.0
- Duty Cycle (D): 0.5
- Fundamental Frequency ( $f_0$ ): 200 Hz
- Harmonic Values:  $z_0 = 20 \exp [j0^\circ]$   
 $z_{-1} = z_1 = 12.3324 \exp [j0^\circ]$   
 $z_{-2} = z_2 = 0.000 \exp [j0^\circ]$   
 $z_{-3} = z_3 = 4.244134 \exp [j180^\circ]$   
 $z_{-4} = z_4 = 0.000 \exp [j0^\circ]$   
 $z_{-5} = z_5 = 2.546479 \exp [j0^\circ]$

## 2. Rectangular-envelope LFM Pulse [Ref. 18]

The complex Fourier coefficients used to synthesize the LFM pulse are found using a procedure similar to that used for the CW pulse except the closed form expression for the complex-valued continuous spectrum of the LFM pulse was found by using the method of stationary phase. Officer [Ref. 20] describes the method of stationary phase as does Papoulis [Ref. 21] who also provides a complete description of the LFM waveform. The following transmit signal parameters were used in all LFM pulse simulations:

- Amplitude (A): 40.0
- Duty Cycle (D): 0.8
- Phase Deviation Constant (B): 2356.2 radians/volt
- Fundamental Frequency (f): 10 Hz

AD-A171 396

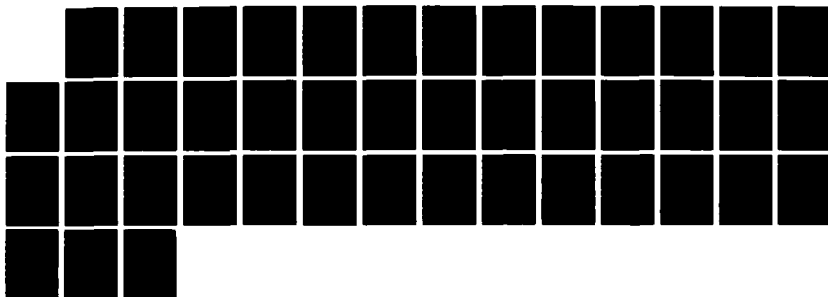
TWO-DIMENSIONAL BEAMFORMING USING A FREQUENCY DOMAIN  
COMPLEX LEAST MEAN-SQUARES (LMS) ADAPTIVE FILTER(U)  
NAVAL POSTGRADUATE SCHOOL MONTEREY CA F CHAN JUN 86

2/2

UNCLASSIFIED

F/G 3/3

ML





- Harmonic Values:  $z_0 = 14.60593 \exp [j45^\circ]$   
 $z_{-1} = z_1 = 14.60593 \exp [j21^\circ]$   
 $z_{-2} = z_2 = 14.60593 \exp [309^\circ]$   
 $z_{-3} = z_3 = 14.60593 \exp [j189^\circ]$

## B. PROBLEM STATEMENT

A pulsed signal (CW or LFM) is sent to an intended receiver in the far-field. The signal at the receive array has a planar wavefront. The direction of arrival of the incident plane wave is determined by applying the frequency domain LMS adaptive filter to phase align (cophase) signals at all sensor elements in the planar array. The discrete time signal at element (m,n) has the form:

$$y(\ell T_s, m d_x, n d_y) = \tilde{z}(\ell T_s) e^{j \frac{2\pi}{\lambda} (u m d_x + v n d_y)} \quad (4.2)$$

where

$$\tilde{z}(\ell T_s) = \sum_{k=-K}^K z_k e^{jk 2\pi f_o t} \quad (4.3)$$

$\ell$ : time index

$m$ : element index in the x-direction

$n$ : element index in the y-direction

$T$ : sampling period

$u$ : direction cosine with respect to the x-axis

v: direction cosine with respect to the y-axis  
 d: interelement spacing in the x-direction  
 d: interelement spacing in the y-direction  
 z: complex Fourier coefficient  
 f: fundamental frequency  
 K: total number of harmonics

[Ref. 5] shows that the number of time samples needed to completely describe equation (4.3) is L, where:

$$L \geq 2K + 1 \quad (4.4)$$

The system parameters are:

	<u>CW</u>	<u>LFM</u>
Integration time ( $T_0$ ):	5 mS	100 mS
Frequency resolution ( $f_0$ ):	200 Hz	10 Hz
Number of samples (L):	11	7
Number of sensors (M):	5	5
Number of sensors (N):	5	5
Sampling rate ( $f_s$ ):	2200 samples per second	70 samples per second
Number of frequency bins (Q):	11	7
Element spacing $d_x, d_y$ :	0.1229 meters	0.1229 meters
Carrier frequency ( $f_c$ ):	5 KHz	5 KHz
Noise model:	Additive white Gaussian noise for both cases	
Number of complex noise samples/pulse:	275	175

The carrier frequency  $f_c$  is assumed to be known a priori. It is found for the CW pulse that the best direction cosine estimates are obtained by processing the spectral line corresponding to the carrier frequency. This is reasonable since the signal-to-noise ratio at that bin is the highest. For the LFM pulse, all the harmonic lines still have roughly the same magnitude after propagating through the medium. The accuracy in estimating the direction cosines is about the same for any harmonic line. Therefore the spectral line corresponding to the carrier is processed.

### C. RESULTS

The homogeneous medium case is considered first for both CW and LFM pulses, followed by the inhomogeneous case.

#### 1. Homogeneous Case

The parameters for the system geometry (Figure 29) are:

Speed of sound ( $c_0$ ): 1475 meters/second  
 Depth of transmit array ( $Y_0$ ): 1000 meters  
 Depth of receive array ( $Y_r$ ): 2500 meters  
 Cross range ( $X_r - X_0$ ): 500 meters  
 Line of sight range  $|r - r_0|$ : 3000 meters  
 True spherical angle  $\theta$ :  $31.81^\circ$   
 True spherical angle  $\phi$ :  $-108.4^\circ$   
 Direction cosine  $u$ : -0.1666  
 Direction cosine  $v$ : -0.5000

The three array configurations of the frequency domain LMS adaptive filter were then applied to the CW and LFM pulse cases to estimate the direction cosines. The averaged results for one pulse corrupted by 100 sample functions of noise at an input SNR of 0 dB at a single array element for the CW pulse, homogeneous case are presented in Table 9. The initial convergence coefficient is 0.5 and the scale factor  $\alpha_s$  is 0.909 for both CW and LFM waveforms.

TABLE 9

PERFORMANCE OF COMPLEX LMS ADAPTIVE FILTER FOR  
SPATIAL RESOLUTION, 100 ITERATIONS, INPUT  
SNR = 0 dB FOR CW PULSE, HOMOGENEOUS CASE

Algorithm			
	orthogonal linear arrays	2-dimensional with separable phase weights	2-dimensional array
u	-0.1666	-0.1666	-0.1666
v	-0.5000	-0.5000	-0.5000
$\hat{u}$	-0.1714	-0.1672	-0.1670
$\hat{v}$	-0.4757	-0.5003	-0.5032
$\Delta u$	-0.00048	-0.0006	-0.0004
$\Delta v$	0.0243	-0.0003	-0.0032
$\epsilon$	0.0247	-0.000624	0.0032
$\theta$	31.81°	31.81°	31.81°
$\phi$	-108.4°	-108.4°	-108.4°
$\hat{\theta}$	30.37°	31.84°	32.02°
$\hat{\phi}$	-109.8°	-108.5°	-108.4°

The rms error versus signal-to-noise ratio curves for all three array configurations are presented in Figure 31.

The simulation results for the LFM pulse in the homogeneous medium at an input SNR of 0 dB at a single array element are summarized in Table 10. A total of 100 different noise sample functions were used to corrupt the received signal. The tabulated values in Table 10 are the ensemble average values. Figure 32 illustrates the rms error versus SNR plot for the LFM pulse in the homogeneous medium.

TABLE 10

PERFORMANCE OF COMPLEX LMS ADAPTIVE FILTER FOR  
SPATIAL RESOLUTION, 100 ITERATIONS, INPUT  
SNR = 0 dB FOR LFM PULSE, HOMOGENEOUS CASE

	Algorithm		
	orthogonal linear arrays	2-dimensional with separable phase weights	2-dimensional array
u	-0.1666	-0.1666	-0.1666
v	-0.5000	-0.5000	-0.5000
$\hat{u}$	-0.1096	-0.1611	-0.1462
$\hat{v}$	-0.2695	-0.4096	-0.4079
$\Delta u$	0.0570	0.0055	0.0204
$\Delta v$	0.2305	0.0904	0.0921
$\epsilon$	0.2375	0.0905	0.0943
$\theta$	31.81°	31.81°	31.81°
$\phi$	-108.4°	-108.4°	-108.4°
$\hat{\theta}$	16.91°	26.11°	25.68°
$\hat{\phi}$	-112.1°	-111.5°	-109.7°

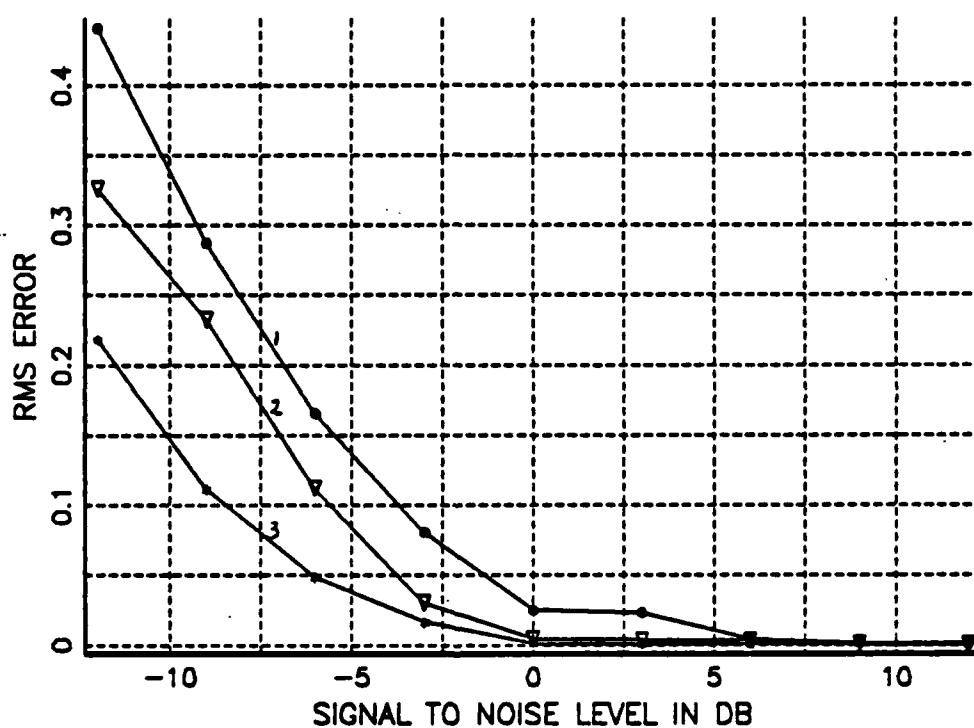


Figure 31. The RMS Error in Estimating  $u$  and  $v$  Versus Input SNR for the CW Pulse/Homogeneous Medium Case.

Curve 1: Orthogonal Linear Arrays Configuration

Curve 2: Two-dimensional Array

Curve 3: Two-dimensional Array with Separable Weights

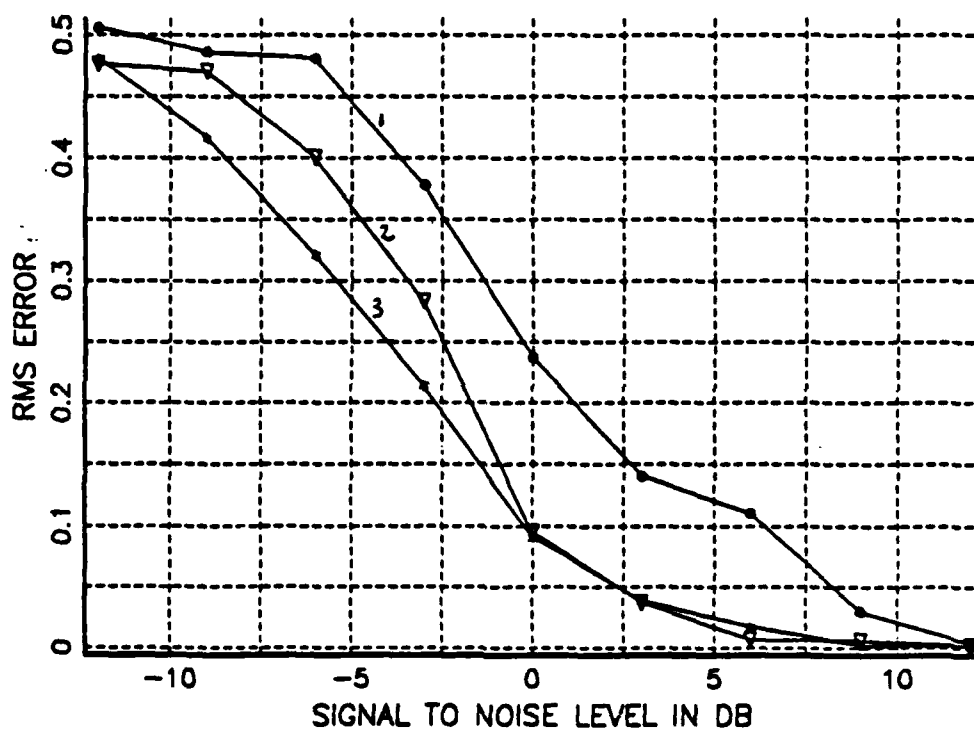


Figure 32. The RMS Error in Estimating  $u$  and  $v$  Versus Input SNR for the LFM Pulse/Homogeneous Medium Case.

Curve 1: Orthogonal Linear Arrays Configuration

Curve 2: Two-dimensional Array

Curve 3: Two-dimensional Array with Separable Weights

The performance of the LFM pulse is worse than that of the CW pulse since the number of samples per pulse is seven where the CW pulse has eleven time samples per pulse. Consider also the Fourier coefficients given in Section A of this chapter. The magnitude of the spectral line corresponding to the carrier for the CW pulse is 1.37 times larger than that of the corresponding spectral line in the LFM pulse. However, for both waveforms, it can be seen from Figures 31 and 32 that the two-dimensional array with separable weights has the best performance, followed by the two-dimensional array and orthogonal linear arrays, respectively. For the CW pulse, accurate spatial localization can be obtained for SNR greater than -3 dB. For the LFM pulse, the SNR required is about 3 dB.

## 2. Inhomogeneous Case [Ref. 18]

The parameters for the system geometry (Figure 32) are:

- Speed of sound ( $c_0$ ): 1475 meters per second
- Gradient: 0.017 per second
- Depth of transmit array ( $Y_0$ ): 1000 meters
- Depth of receive array ( $Y_r$ ): 2500 meters
- Cross range ( $X_r - X_0$ ): 500 meters
- Line of sight range  $|r - r_0|$ : 3000 meters
- True spherical angle  $\theta$ :  $30.10^\circ$
- True spherical angle  $\phi$ :  $-109.4^\circ$
- Direction cosine  $u$ : -0.1666
- Direction cosine  $v$ : -0.4731

Figure 30 shows that the path traveled by the acoustic rays is bent. The LMS adaptive filter is able to resolve the actual direction of arrival but not the true line of sight direction to the transmit array. The initial convergence coefficient  $\mu$  is set equal to 0.5 and the scale factor  $\alpha_s$  is set equal to 0.909. Both the CW and LFM pulses are considered for each of the three array configurations. Table 11 summarizes the performance of the LMS adaptive filter applied to the CW pulse case at an input SNR of 0 dB at a single array element. Figure 33 shows the decline of rms error as the signal-to-noise ratio is increased. All three array configurations are included in the plot for comparison.

The performance for the LFM pulse case is tabulated in Table 12 for an input SNR of 0 dB at a single array element. Figure 34 illustrates the performance of all three array configurations versus signal-to-noise ratio for the LFM pulse case.

#### D. SUMMARY

For both the homogeneous and inhomogeneous medium cases, the complex LMS adaptive filter performed as expected. The array configuration that assumed separability of the complex weights consistently demonstrated better performance than that of the orthogonal linear arrays and the two-dimensional array. The superior performance can be attributed to the fact that equation (2.24) which describes the reception of a plane wave by a planar array is separable. Therefore, by

TABLE 11

PERFORMANCE OF COMPLEX LMS ADAPTIVE FILTER FOR  
 SPATIAL RESOLUTION, 100 ITERATIONS, INPUT  
 SNR = 0 dB FOR CW PULSE, INHOMOGENEOUS CASE

	Algorithm		
	orthogonal linear arrays	2-dimensional with separable phase weights	2-dimensional array
u	-0.1666	-0.1666	-0.1666
v	-0.4731	-0.4731	-0.4731
$\hat{u}$	-0.1663	-0.1686	-0.1651
$\hat{v}$	-0.4527	-0.4782	-0.4746
$\Delta u$	0.0003	-0.0019	0.0015
$\Delta v$	0.0204	-0.0051	-0.0015
$\epsilon$	0.0204	0.0054	0.0022
$\theta$	30.10°	30.10°	30.10°
$\phi$	-109.4°	-109.4°	-109.4°
$\hat{\theta}$	28.83°	30.47°	30.17°
$\hat{\phi}$	-110.2°	-109.4°	-109.2°

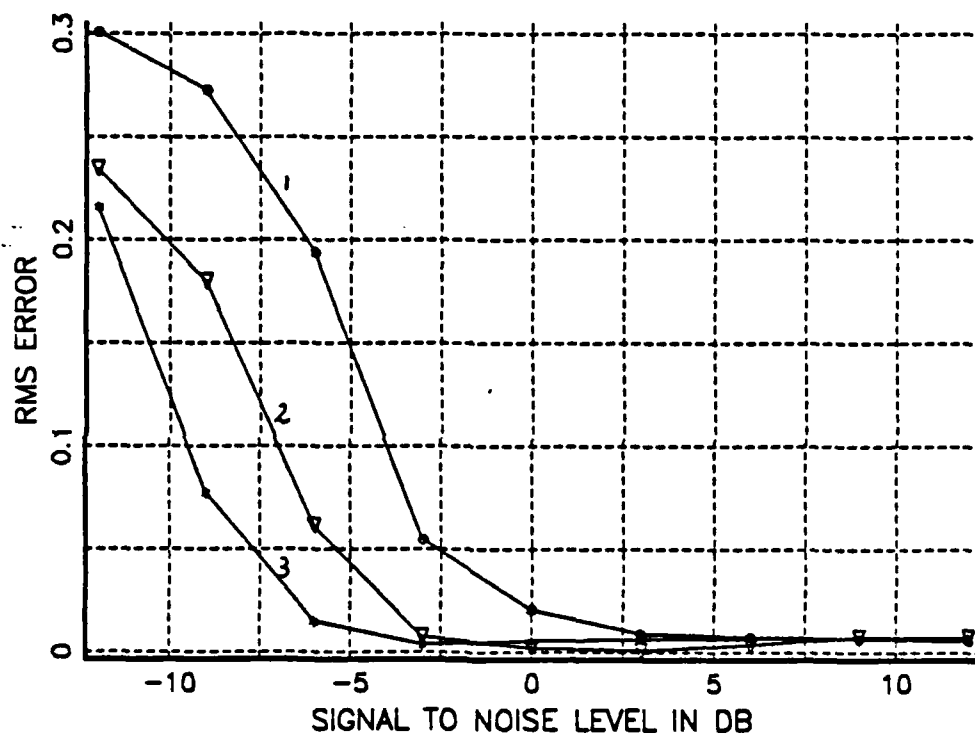


Figure 33. The RMS Error in Estimating  $u$  and  $v$  Versus Input SNR for the CW Pulse/Inhomogeneous Medium Case.

Curve 1: Orthogonal Linear Arrays Configuration

Curve 2: Two-dimensional Array

Curve 3: Two-dimensional Array with Separable Weights

TABLE 12

PERFORMANCE OF COMPLEX LMS ADAPTIVE FILTER FOR  
 SPATIAL RESOLUTION, 100 ITERATIONS, INPUT  
 SNR = 0 dB, LFM PULSE, INHOMOGENEOUS CASE

	Algorithm		
	orthogonal linear arrays	2-dimensional with separable phase weights	2-dimensional array
u	-0.1666	-0.1666	-0.1666
v	-0.4731	-0.4731	-0.4731
$\hat{u}$	-0.1035	-0.1614	-0.1417
$\hat{v}$	-0.2447	-0.4058	-0.3332
$\Delta u$	0.0631	0.0052	0.0249
$\Delta v$	0.2284	0.0673	0.1399
$\epsilon$	0.2369	0.0675	0.1421
$\theta$	30.10°	30.10°	30.10°
$\phi$	-109.4°	-109.4°	-109.4°
$\hat{\theta}$	15.41°	25.89°	21.23°
$\hat{\phi}$	-112.93°	-111.7°	-113.0°

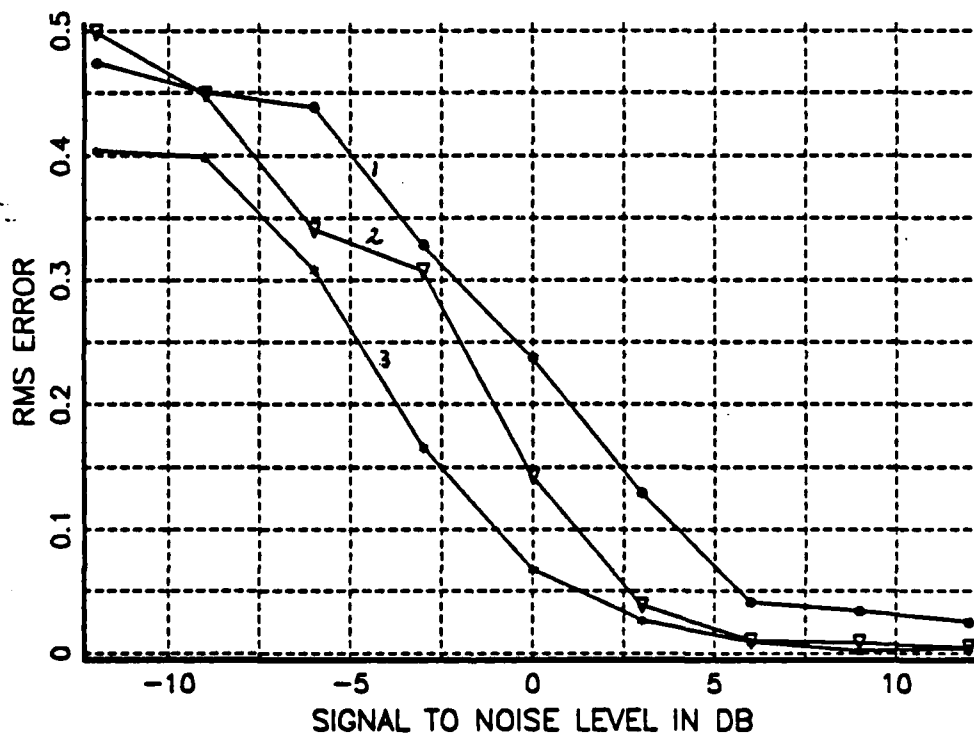


Figure 34. The RMS Error in Estimating  $u$  and  $v$  Versus Input SNR for the LFM Pulse/Inhomogeneous Medium Case.

- Curve 1: Orthogonal Linear Arrays Configuration
- Curve 2: Two-dimensional Array
- Curve 3: Two-dimensional Array with Separable Weights

assuming separable complex weights, the system is set up to match the physics of the problem. The performance of this pulse communication system can be enhanced by increasing the pulse width, taking more time samples per unit time, using high resolution spectrum analysis, and enlarging the size of the array by adding more sensor elements.

## V. CONCLUSIONS AND RECOMMENDATIONS

The frequency domain LMS adaptive algorithm has been shown to perform the function of spatial resolution. The number of iterations required (approximately 35) to reach a steady state is found to be much fewer than that of a comparable time domain adaptive filter [Refs. 2,4]. The three modifications made to the original complex LMS adaptive filter [Refs. 1,4] are:

- normalization of the complex weights to unity magnitude after each update
- reduction of the magnitude of the convergence coefficient for each iteration
- unwrapping of the phase weights

It has been shown that the above three modifications enable the frequency domain LMS adaptive filter to be applied to a multiple element array, to have a fast convergence rate and robustness, and to cover the entire angular range of  $\theta$  and  $\phi$  values.

In Chapter III, a passive low-frequency signal was generated to test the performance of the frequency domain LMS adaptive filter in the presence of white Gaussian noise. The low frequency problem is significant in the area of long range detection and possibly long range control and communication for ballistic missile submarines. Some form of modulation, whether amplitude or angle, will have to be used

to carry the information. The slow data rate is not a major drawback since only certain predefined emergency operation codes will be transmitted. The simulation results indicate that for an input SNR at a single array element of greater than -3 dB, accurate bearing and depressive angle estimates can be obtained.

In Chapter IV, a pulse communication problem was considered. Two types of pulses, rectangular-envelope CW and rectangular-envelope LFM pulses, were used. The possible applications at this frequency range (5 KHz) are high resolution SONAR imaging, active SONAR detection, and communication-between submerged vessels. The performance of the frequency domain LMS adaptive filter was again tested in the presence of white Gaussian noise. The simulation results indicate that accurate bearing and depression angle estimates can be obtained for input SNRs of greater than 0 dB. The result here is slightly worse than that of the passive low-frequency case due to the shorter data length used for the pulse communication waveforms. For the simulations in Chapter IV, the number of time samples collected is the minimum required to satisfy the Nyquist sampling theorem.

The following three configurations of the frequency domain LMS adaptive filter were considered:

- orthogonal linear arrays
- two-dimensional array with separable phase weights
- two-dimensional array

In all simulations, the configuration that used the separability assumption produced the best results. This is quite reasonable since this configuration uses all the output data from the available elements and more importantly, its assumption of separability matches the physics of the plane wave signal since the phases of a plane wave in the orthogonal x and y directions are separable.

In the course of this investigation, some interesting topics for further research revealed themselves:

- exact target localization (range, depth, bearing, and depression angle) if accurate environmental data can be obtained
- more efficient update algorithm for the convergence coefficient
- implementation of more efficient software
- application of the steady state phase weights generated by the frequency domain LMS adaptive filter to Blount's [Ref. 18] correlator receiver
- addition of a noise reduction system before spectral estimation
- modifications to make the system jam-resistant
- applications of other high resolution spectral analysis techniques to produce frequency spectra (such as maximum entropy [Ref. 22], autoregressive, maximum likelihood, etc.).

## APPENDIX A

### THE FREQUENCY DOMAIN LMS ADAPTIVE ALGORITHM

#### A. DERIVATION

Consider the phase aligning system shown in Figure 13. The performance objective is for the adaptive filter to converge to a set of phase weights such that the array output signal will match a reference signal. In the frequency domain, the output of a linear array of  $M$  elements at iteration  $i$  can be written as:

$$\hat{z}_i(q) = \frac{1}{M} \sum_m c_i(m) Y(q, m) = \frac{1}{M} \underline{c}_i^T \underline{Y}(q) \quad (A.1)$$

If  $Z(q)$  is the reference signal, then the error between the reference and the array output is:

$$e_i = Z(q) - \hat{z}_i(q) \quad (A.2)$$

where  $e_i$  is a complex quantity.

The mean square error is:

$$e_i e_i^* = |e_i|^2 = [Z(q) - \hat{z}_i(q)][Z(q) - \hat{z}_i(q)]^* \quad (A.3)$$

$$|e_i|^2 = |Z(q)|^2 - \hat{z}_i(q) Z^*(q) - \hat{z}_i^*(q) Z(q) + |\hat{z}_i(q)|^2 \quad (A.4)$$

Substituting equation (A.1) into equation (A.4) for  $z_i(q)$  yields:

$$|e_i|^2 = |z(q)|^2 - z^*(q) (\underline{c}_i^T \underline{y}(q)) - z(q) (\underline{c}_i^T \underline{y}(q))^* + |\underline{c}_i^T \underline{y}(q)|^2 \quad (A.5)$$

The complex weight vector that will minimize equation (A.5) is computed from the following recursive algorithm [Refs. 1, 6,14]:

$$\underline{c}_{i+1} = \underline{c}_i + 2\mu_i e_i \underline{y}^*(q) \quad (A.6)$$

where  $\mu_i$  is the convergence coefficient used in the gradient method [Ref. 6].

For the two-dimensional case discussed in Chapter II, Section 3.b, replace  $\underline{c}_{i+1}$  with  $\underline{cd}_{i+1}$  to yield:

$$\underline{cd}_{i+1} = \underline{cd}_i + 2\mu_i e_i \underline{y}^*(q) \quad (A.7)$$

where:

$$e_i = z(q) - \frac{1}{MN} \sum_m \sum_n \underline{cd}_i(m,n) Y(q,m,n) \quad (A.8)$$

If the complex weights  $\{\underline{cd}_i(m,n)\}$  are separable, then

$$\underline{cd}_i(m,n) = c_i(m) d_i(n)$$

and:

$$\underline{c}_{i+1}(m) = \underline{c}_i(m) + 2u_i e_i \left( \sum_n d_i(n) Y(q, m, n) \right)^* \quad (A.9)$$

$$\underline{d}_{i+1}(m) = \underline{d}_i(n) + 2 \sum_i e_i \left( \sum_m c_i(m) Y(q, m, n) \right)^* \quad (A.10)$$

where:

$$e_i = Z(q) - \frac{1}{MN} \sum_m c_i(m) \sum_n d_i(n) Y(q, m, n) \quad (A.11)$$

Reference 4 studied the application of the frequency domain LMS algorithm to a split array. The error signal is the difference between the outputs of the two arrays. It is possible to extend this idea to an  $(M \times N)$  planar array by generating an error signal  $e_i(m, n)$  at each element location where:

$$e_i(m, n) = Z(q) - c d_i(m, n) Y(q, m, n) \quad (A.12)$$

for all  $m, n$ . Although this scheme is not studied in this thesis, the implementation is rather straightforward. One needs only to replace the error  $e_i$  with  $e_i(m, n)$  in all the equations and to rewrite the code to generate the error. This scheme, however, does not have the advantage of averaging noisy data points from all of the elements in the

array to come up with an estimate. Therefore, it can be assumed that the noise performance will probably be inferior.

The magnitude of the reference signal  $Z(q)$  is generated by averaging all  $(M \times N)$  magnitude spectra whereas the phase of  $Z(q)$  is taken to be the phase of the reference element. A thresholding is done to determine which frequency bins should be processed.

#### B. MODIFICATION TO THE LMS ADAPTIVE ALGORITHM TO MAKE IT USEFUL FOR SPATIAL RESOLUTION

Three modifications are incorporated in the basic LMS adaptive algorithm.

##### 1. Normalization of Recursive Complex Weights

The components of the recursive complex weights ( $\underline{c}_i$ ,  $\underline{d}_i$  and  $\underline{cd}_i$ ) must be normalized to have magnitudes equal to one. This restriction forces the algorithm to achieve minimum error by adjusting the phase weights only. The estimation of direction cosines depends on the linear relationship of the phases of the signal across the array. Figure 35 shows that, without the normalization performed after each complex weight update, the vector sum composing the estimate can be made close to that of the reference. The correct values of the direction cosines can only be achieved if each component in equation (A.1) has the same phase as the reference phasor. All the vector sums shown in Figure 35 have the same resultant phase and magnitude as the reference but the phases of the components are not equal. It can also be

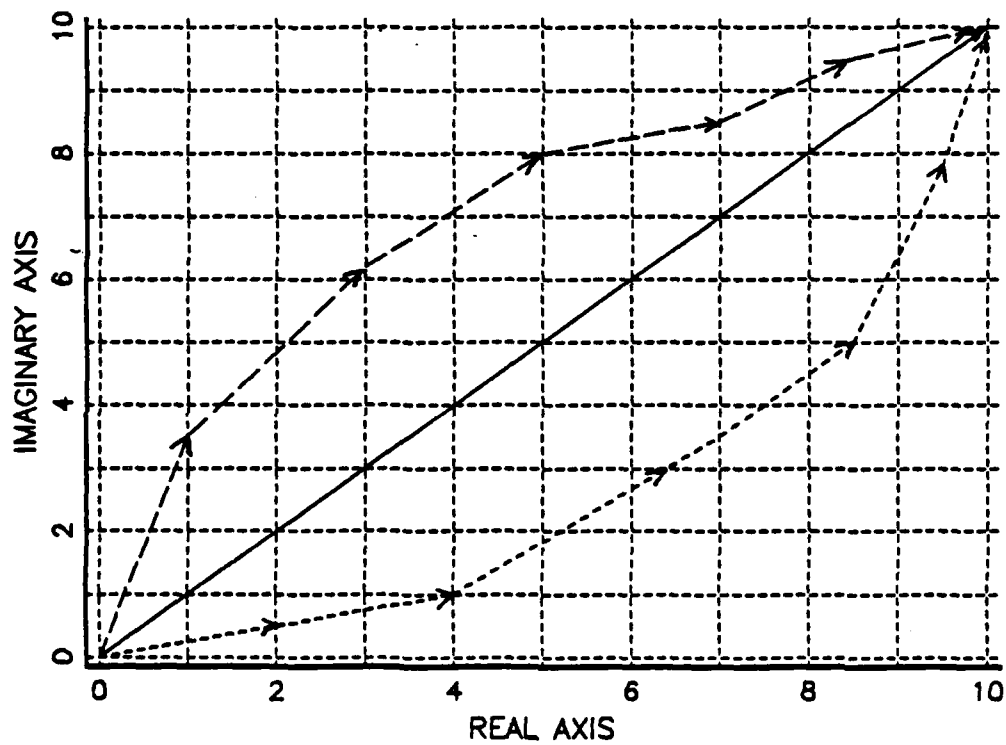


Figure 35. Different Ways of Adding Up Vectors to Obtain the Same Resultant

seen that there are infinitely many ways to achieve a small error without the normalization. The LMS adaptive filter implemented for this thesis has a unity magnitude across the array. It is, in fact, a phase-only filter. With the normalization, each component is forced to adapt to the phase angle of the reference. This is the only way that spatial resolution (based on the amount of phasor rotation of adaptive weights) can be achieved.

## 2. The Convergence Coefficient ( $\mu$ )

This quantity is sometimes referred to as the feedback coefficient, signifying the analogy to control systems [Ref. 6]. For nonstationary environments, a constant convergence coefficient is usually chosen [Refs. 1,4,23]. However, if stationarity can be assumed, the performance of the LMS adaptive filter can be improved by using a monotonically decreasing scheme for implementing the convergence coefficient [Ref. 11]. If a constant convergence coefficient is used, the bound on the choice of value is given by [Refs. 12,24]:

$$0 < \mu < \lambda_{\max}^{-1} \quad (\text{A.13})$$

where

$$\lambda_{\max} < \text{Tr}[R] = \sum_{i=0}^I R(i,i) = \sum_{i=0}^I R(0) = (I+1)R(0)$$

and  $R$  is the covariance matrix of the received noise corrupted signal. If  $\mu$  is larger than the maximum determined by equation (A.13), oscillation will occur [Ref. 25] and the LMS adaptive filter will not converge. If  $\mu$  is too small, then the rate of convergence is slow. Figures 36, 37 and 38 show the convergence characteristics for different values of  $\mu$ .

The recursive LMS algorithm is based on the stochastic approximation technique [Ref. 11]. The choice of  $\mu$  is optimal if the following conditions are met [Ref. 12]:

$$\mu_i > 0$$

$$\lim_{i \rightarrow \infty} \mu_i = 0$$

$$\sum_{i=1}^{\infty} \mu_i = \infty$$

$$\sum_{i=1}^{\infty} \mu_i^2 < \infty$$

A particular choice of  $\mu_i$  that meets the above four conditions is  $\mu_i = 1/i$  [Ref. 12]. The effect of the adaptation decreases with the number of iterations and ceases completely for large  $i$ . Simulations show that the above choice of  $\mu_i$  is better than using a constant  $\mu$ , however, the choice

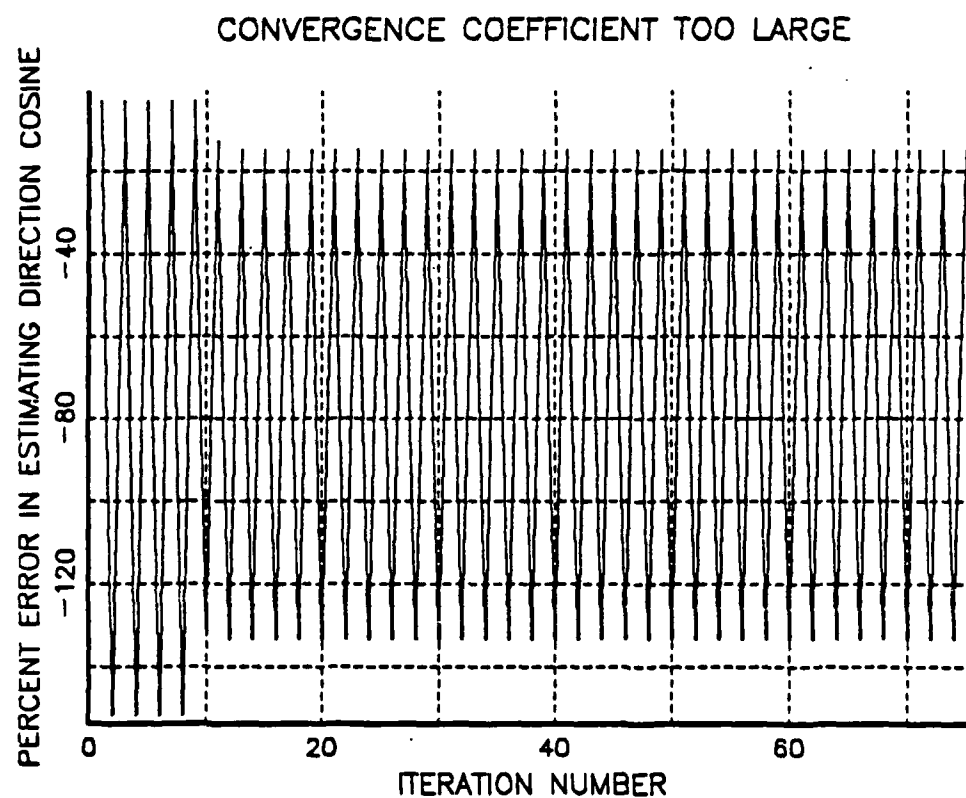


Figure 36. Convergence Coefficient (Constant Value)  
Too Large

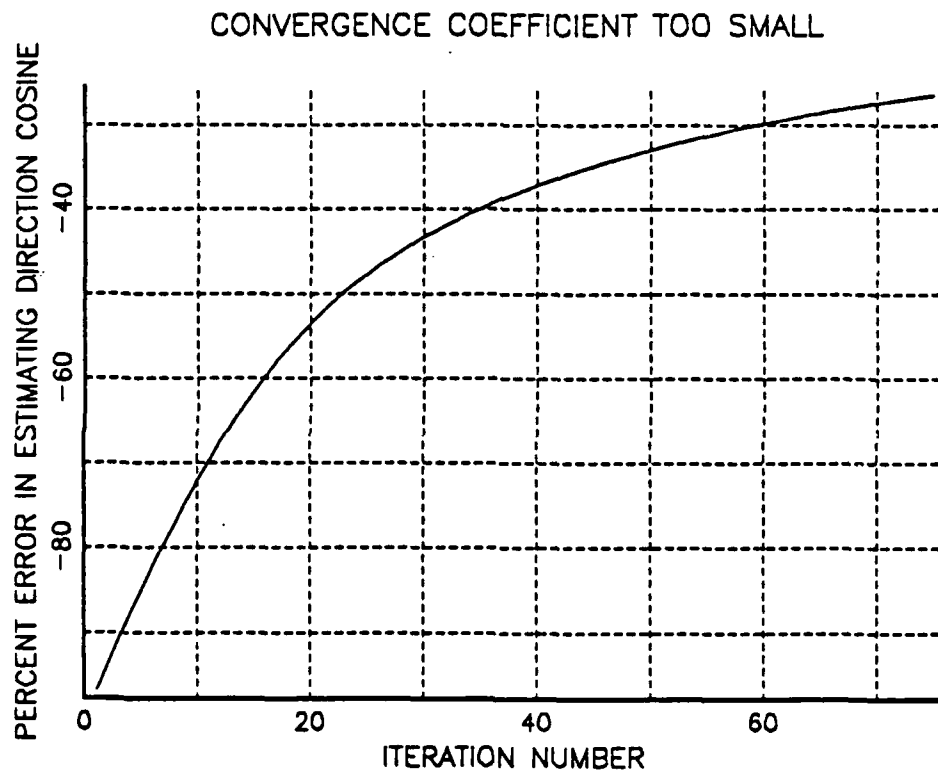


Figure 37. Convergence Coefficient (Constant Value) Too Small

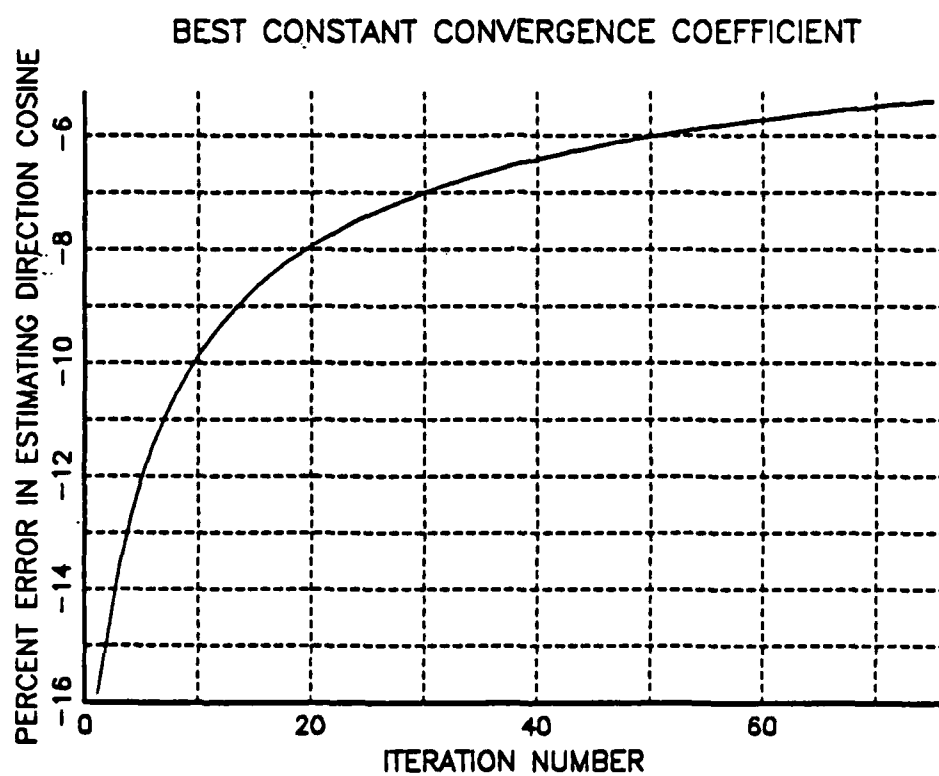


Figure 38. Optimum Convergence Coefficient  
(Constant Value)

$$\mu_i = \alpha_s^i \mu_0 \quad (\text{A.14})$$

where  $0 < \alpha_s < 1$  and  $\mu_0$  is the initial value, appears to speed the rate of convergence and also achieve a high degree of accuracy. Equation (A.14) does not meet the condition  $\sum_{i=1}^{\infty} \mu_i = \infty$ , but simulations show that the response of the LMS adaptive filter is fast and accurate for  $0.75 < \alpha_s < 0.95$ . Further investigations of the convergence characteristics are warranted. The current implementation of the convergence coefficient results from experimentation with various values of  $\alpha_s$  to achieve the best estimates of direction cosines. With this scheme, the initial value of  $\mu_i$  can be set quite liberally since the value of  $\mu_i$  decreases geometrically.

### C. PHASE WRAP-AROUND PROBLEM

The resolution of the phase wrap-around problem in the adaptive phase weights was discussed in Chapter II extensively. The scheme to resolve the phase ambiguity depends on the proper functioning of the elements adjacent to the reference element. In the event that some of those adjacent elements are not operational, the unwrapping scheme will have degraded performance. However, since the reference element can be any element in the array, it is possible to shift the location of the reference element to a region of the array that has sufficient adjacent elements that are functioning properly.

## APPENDIX B

### DESCRIPTION OF SIMULATION PROGRAM FOR THE PASSIVE DETECTION CASE

The VS APL application package worksapce (CMS file ADAPTIVE VSAPLWS) contains all the functions necessary to implement the simulation discussed in Chapter III. The general processing flow is as follows:

- generate time samples of a plane wave signal of frequency  $f$  incident upon a  $(M \times N)$  planar array with angles of incidence  $(\theta, \phi)$
- add white Gaussian noise for a desired SNR
- compute the discrete Fourier transform (DFT) of each of the  $M \times N$  time sequences
- determine the spectral line with the largest magnitude and its corresponding frequency bin number
- apply one of the three frequency domain LMS adaptive filters (orthogonal linear arrays, two-dimensional array with separable complex weights, or two-dimensional array)
- compute estimates of direction cosines.

Usage of the functions are described below.

#### A. SIG2D

SIG2D generates planar array signal at each element location (equation (2.28)):

Syntax:  $YN \leftarrow AG1 \text{ SIG2D } AG2$

$YN$  is a  $L \times M \times N$  matrix where  $L$  is the number of time samples,  $M$  is the number of elements in the x-direction, and

N is the number of elements in the y-direction. AG1 is the spherical angle  $\theta$  and AG2 is the spherical angle  $\phi$ . The speed of sound (c), the signal amplitude (A), the frequency of the signal (F), the interelement spacing (DX and DY), the sampling interval (T), the number of elements (M,N) and the number of time samples (L) can be changed by editing the function.

#### B. NORRAND

NORRAND generates independent white Gaussian noise samples.

Syntax: NOISE  $\leftarrow$  K NORRAND N N1

K is the number of noise samples desired, N is the mean N1 is the variance. The noise array NOISE must be reshaped to conform to the shape of the signal generated by SIG2G by:

NOISE  $\leftarrow$  L M N  $\rho$  NOISE

The standard deviation  $\sigma_N = 1$  is necessary to scale a sample function of noise with zero mean and variance 1 to a desired signal-to-noise ratio. The signal power at each element is  $A^2/2$  and the noise power at each element is  $\sigma_N$ . The input signal-to-noise ratio at a single array element is then given by:

$$\text{SNR} = \frac{A^2/2}{\sigma_N^2} = \frac{A^2}{2\sigma_N^2} \quad (\text{B.1})$$

Solving for  $\sigma_N$  yields:

$$\sigma_N = \left( \frac{A^2}{2(\text{SNR})} \right)^{1/2} \quad (\text{B.2})$$

where A is the amplitude of the signal and SNR is the numerical signal-to-noise ratio. Therefore, a noisy signal with the desired SNR can be generated as:

$$\text{RN} \leftarrow \text{YN} + \sigma_N \times \text{NOISE} \quad (\text{B.3})$$

where NOISE has zero mean and variance 1.

### C. DFTWRT

DFTWRT computes the discrete Fourier transform with respect to the time index for each element (equation (2.42)).

Syntax:  $\text{YK} \leftarrow \text{DFTWRT RN}$

YK has dimensions  $L \times M \times N$ ; the first index L is now the total number of frequency bins. RN is the noisy signal generated by adding noise to the output of SIG2D. A total of  $(M \times N)$  L-point DFTs are computed using a radix-2 FFT algorithm.

#### D. ADPLMS

ADPLMS computes estimates of the direction cosines using the frequency domain LMS algorithm for the orthogonal array configuration.

Syntax: QTGT ADPLMS YK

QTGT is the frequency bin number where a valid signal has been identified and YK is the output of the function DFTWRT. A reference signal at frequency bin QTGT is generated by calling the function REFGEN. Direction cosine estimates  $u$  and  $v$  are computed in two different loops since in general the number of elements  $M$  is not necessarily equal to  $N$ . Estimates of both direction cosines are generated for each iteration under the names UHAT and VHAT. The phase unwrapping is done by calling the function DC1DX for the x-direction and DC1DY for the y-direction. The number of iterations (ITER) and the initial convergence coefficients (MUX, MUY) can be changed by editing the function ADPLMS. The scale factor (SCMU) for decreasing the convergence coefficients can be changed in the workspace.

#### E. QFLMS

QFLMS computes estimates of the direction cosines using the frequency domain LMS algorithm for the two-dimensional planar array with separable complex weights.

Syntax: QTGT QFLMS YK

QTGT is the frequency bin number and YK is the output of the function DFTWRT. A reference signal is generated by the function REFGEN. Direction cosine estimates u and v are computed every iteration of the LMS adaptive loop. They are stored in the vectors named UHATQF and VHATQF. The phase unwrapping is done by using DC1DX and DC1DY in the x and y-directions, respectively. Recall that only M+N complex weights are updated for this configuration because of the separability assumption. The initial convergence coefficient (MUQ) and the number of iterations (ITER) can be changed by editing the function QFLMS. The scale factor is named SCMU and is stored in the variable list in the workspace.

#### F. ADPLMS2D

ADPLMS2D computes estimates of the direction cosines using the frequency domain LMS adaptive algorithm for a two-dimensional planar array.

Syntax: QTGT ADPLMS2D YK

QTGT and YK are the same quantities described in the last two functions. A reference signal at frequency bin QTGT is generated. Direction cosine estimates u and v are computed for each iteration and stored in vectors named UHAT2D and VHAT2D. The phase unwrapping is accomplished by using

the function DC2D. The number of iterations (ITER) and the initial convergence coefficient (MUG) can be changed by editing the function ADPLMS2D. The scale factor can be changed by assigning a different value to SCMU in the workspace. The use of a different unwrapping function is required since the complex weights are not assumed to be separable.

#### G. REFGEN

REFGEN generates a reference signal at a particular frequency bin QTGT.

Syntax: CQREF ← QTGT REFGEN YK

CQREF is the reference signal used in the frequency domain LMS adaptive filter. The magnitude of CQREF is obtained by averaging the magnitudes of all ( $M \times N$ ) frequency spectra in the frequency bin QTGT. The phase of CQREF is taken to be the phase of the reference element in the QTGT frequency bin.

#### H. DC1DX

DC1DX unwraps the phase weights for a linear array in the x-direction.

Syntax: UHAT[i] ← N DC1DY DV

UHAT[i] is the direction cosine estimate  $u$  of the  $i^{\text{th}}$  iteration,  $M$  is the number of elements in the  $x$ -direction and  $CV$  is a complex vector of  $M$  phase weights that will cophase the incident signal.

#### I. DC1DY

DC1DY unwraps the phase weights for a linear array in the  $y$ -direction.

Syntax: VHAT[i]  $\leftarrow$  N DC1DY DV

VHAT[i] is the direction cosine estimate  $v$  of the  $i^{\text{th}}$  iteration,  $N$  is the number of elements in the  $y$ -direction and  $CV$  is a complex vector of  $N$  phase weights that will cophase the incident signal.

#### J. DC2D

DC2D unwraps the phase weights for a two-dimensional array.

Syntax: DC2D CD

CD is the two-dimensional phase matrix that will cophase the incident plane wave signal. This function is used by the function ADPLMS2D.

An example of using this application package is shown as follows:

- YN ← 55 SIG2D 35	signal generation
- NOISE ← 3200 NORRAND 0 1	noise generation
- NOISE ← 128 5 5 ρ NOISE	noise generation
- RN ← YN + SCALE NOISE	noisy signal
- YK ← DFTWRT RN	transform to frequency domain
- QTGT ADPLMS YK	estimate direction cosines
- QTGT ADPLMS2D YK	estimate direction cosines
- QTGT QFLMS YK	estimate direction cosines

This sequence of statements generates a plane wave signal incident upon a  $5 \times 5$  planar array with angles of incidence  $\theta = 55^\circ$  and  $\phi = 35^\circ$ . The number of time samples for each element is 128. A noise matrix is then generated and added to the plane wave signal and the discrete Fourier transform with respect to time is taken for each element in the array. The three array configurations for the frequency domain LMS algorithm are then used sequentially to estimate the direction cosines of the incident plane wave.

## APPENDIX C

### DESCRIPTION OF SIMULATION PROGRAM FOR THE PULSE COMMUNICATION CASE

The VS FORTRAN programs were written to implement the pulse communication problem discussed in Chapter IV. Two separate programs were written utilizing essentially the same subprograms. These programs handle the quadrature demodulated complex envelope signals generated by Vos'[Ref. 19] program. The programs are available on user account 0218P at the Naval Postgraduate School, Monterey, California.

#### A. PROGRAM ADBFM

This program is compiled using FORTVS and is designed to run under DISSPLA. It requires a storage capacity of 1 Mbyte. The following sequence of commands should be used to run the program.

- DEFINE STORAGE 1 M
- I CMS
- GLOBAL TXTLIB VALTLIB VFORTLIB CMSLIB IMSLSP NONIMSL
- GLOBAL LOADLIB VFLODLIB
- FILEDEF 04 DISK fname DATA  
(fname is the filename of the data file)
- LOAD ADBFM
- DISSPLA ADBFM

When execution begins, the user will be prompted to enter the desired values for the necessary parameters. These

parameters are noise status, input signal-to-noise ratio in dB at a single array element, number of iterations, spectral line to be processed, convergence coefficient, scale factor for the convergence coefficient, and the choice of one of the three array configurations.

For each array configuration, plots of the estimates of the direction cosines are generated. The plots for magnitude and phase of the difference between the reference signal and the estimate are also generated.

#### B. PROGRAM ERVSDB

This program computes the rms errors for various input signal-to-noise ratios. If a plot of rms error versus SNR (dB) is not required, this program does not have to be run under DISSPLA. The following sequence should be used:

- DEFINE STORAGE 1 M (if plot is required)
- I CMS
- GLOBAL TXTLIB VALTLIB VFORTLIB CMSLIB IMSLSP NONIMSL
- FILEDEF 04 DISK fname DATA  
(fname is the filename of the data file)
- LOAD ERVSDB
- DISSPLA ERVSDB (if plot is needed)  
or START \* (if plot is not needed)

When execution begins, the program will prompt the user to enter an initial input signal-to-noise ratio in dB at a single array element. It will then ask for a dB step size such that the next SNR is determined by the current SNR in dB plus the dB step size. A total of nine SNRs are allowed.

For example, if the initial SNR is -12 dB and the step size is 3 dB, then the program will compute rms errors for the set of dB levels {-12, -9, -6, -3, 0, 3, 6, 9, 12}. The other parameters such as iteration number, initial convergence coefficient, scale factor for convergence coefficient, and the spectral line to be processed are entered when prompted. The program will then ask for how many sample functions of signal and noise are to be averaged. Simulation results show that the average of 50 to 100 sample functions are sufficient to reduce the variance of the direction cosine estimates. One of the three array configurations is then chosen by the user to estimate the direction cosines.

The screen output of this program is ordered pairs of rms errors corresponding to a particular input SNR in dB for all nine specified SNRs. A plot of rms error versus SNR in dB can be generated if desired (provided that the program is run under DISSPLA).

### LIST OF REFERENCES

1. Widrow, B., McCool, J., and Ball, M., "The Complex LMS Algorithm," Proc. IEEE, April 1975.
2. Widrow, B., "Adaptive Filters," In: Aspects of Network and System Theory, Dalman, R. and DeClanis, N., Eds. New York: Holt, Rinehart and Winston, 1971.
3. Dentino, M., McCool, J. and Widrow, B., "Adaptive Filtering in the Frequency Domain," Proc. IEEE, Vol. 66, December 1978.
4. Reed, F.A., Feintuch, P.L., and Benshad, N.J., "The Application of Frequency Domain LMS Adaptive Filter to Split Array Bearing Estimation with a Sinusoidal Signal," IEEE Transactions on Acoustics, Speech, and Signal Processing, Vol. ASSP-33, No. 1, February 1985.
5. Ziomek, L.J., Underwater Acoustics--A Linear Systems Theory Approach, Academic Press, 1985.
6. Monzingo, R.A. and Miller, T.W., Introduction to Adaptive Arrays, Wiley, 1980.
7. Knight, W.C., Pridham, R.G. and Kay, S.M., "Digital Signal Processing for SONAR," Proc. IEEE, Vol. 69, No. 11, November 1981.
8. Mucci, R.A., "A Comparison of Efficient Beamforming Algorithms," IEEE Trans. Acoustics, Speech, and Signal Processing, Vol. ASSP-32, No. 3, June 1984.
9. Oppenheim, A.V., ed., Applications of Digital Signal Processing, Prentice Hall, Inc., 1978.
10. Goodman, J.W., Introduction to Fourier Optics, McGraw Hill, 1968.
11. Robbins, H. and Monro, S., "A Stochastic Approximation Method," Ann. Math. Statistics, Vol. 22, No. 1, 1951.
12. Stark, H. and Tuteur, F.B., Modern Electrical Communications Theory and Systems, Prentice Hall, Inc., 1979.
13. Devore, J.L., Probability and Statistics for Engineering and the Sciences, Brooks/Cole, 1982.
14. Frost, O.L., "An Algorithm for Linearly Constrained Adaptive Array Processing," Proc. IEEE, Vol. 60, August 1972.

15. Widrow, B., Montey, P., Griffiths, L. and Goode, B., "Adaptive Antenna Systems," Proc. IEEE, Vol. 55, December 1967.
16. Oppenheim, A.V. and Schaffer, R.W., Digital Signal Processing, Prentice Hall, Inc., 1975.
17. Stremmler, F.G., Introduction to Communication Systems, Addison Wesley, 1982.
18. Blount, R.J. Jr., Underwater Acoustic Model-Based Signal Processing Applied to the Detection of Signals From a Planar Array of Point Source Elements, Master's Thesis, Naval Postgraduate School, Monterey, California, September 1985.
19. Vos, J., Linear Time-Invariant, Space-Invariant Filters and the WKB Approximation with Applications to Underwater Signal Processing, Master's Thesis, Naval Postgraduate School, Monterey, California, December 1984.
20. Officer, C.B., Introduction to the Theory of Sound Transmission, McGraw Hill, 1958.
21. Papoulis, A., Signal Analysis, McGraw Hill, 1977.
22. Skinner, D.P., Hedlicka, S.M. and Matthews, A.D., "Maximum Entropy Array Processing," J. Acoust. Soc. Am., Vol. 66, No. 2, August 1979.
23. Widrow, B. et al., "Stationary and Nonstationary Learning Characteristics of the LMS Adaptive Filter," Proc. IEEE, Vol. 64, August 1976.
24. Orfanidis, S.J., Optimum Signal Processing: An Introduction, MacMillan, 1985.
25. Feuer, A. and Weinstein, E., "Convergence Analysis of LMS Filters with Uncorrelated Gaussian Data," IEEE Trans. Acoustic Speech and Signal Processing, Vol. ASSP-33, No. 1, February 1985.

INITIAL DISTRIBUTION LIST

	No. Copies
1. Defense Technical Information Center Cameron Station Alexandria, Virginia 22304-6145	2
2. Library, Code 0142 Naval Postgraduate School Monterey, California 93943-5000	2
3. Associate Professor L.J. Ziomek, Code 62Zm Department of Electrical and Computer Engineering Naval Postgraduate School Monterey, California 93943-5000	6
4. Associate Professor C.W. Therrien, Code 62Ti Department of Electrical and Computer Engineering Monterey, California 93943-5000	1
5. LT F. Chan c/o Commanding Officer Naval Underwater Systems Center Newport, Rhode Island 02841-5067	1
6. Mr. Charles Stuart DARPA 1400 Wilson Blvd. Arlington, Virginia 22209	1
7. LT F. Chan Naval Underwater Systems Center Detachment New London, Connecticut 06340	2

END

5-87

DTic